Conformation and vibrational spectroscopic analysis of 2,6-bis (4-fluorophenyl)-3,3-dimethylpiperidin-4-one (BFDP) by DFT method: A potent anti-Parkinson's, anti-lung cancer, and anti-human infectious agent

Thangamani Arumugam [a,b,**], Arulraj Ramalingam [c,*], Ahlam Roufieda Guerroudj [d,***], Sivakumar Sambandam [e,f], Nourdine Boukabcha [d,g], Abdelkader Chouaih [d]

[a] *Department of Chemistry, Karpagam Academy of Higher Education, Coimbatore 641 021, Tamil Nadu, India*
[b] *Centre for Material Chemistry, Karpagam Academy of Higher Education, Coimbatore 641 021, Tamil Nadu, India*
[c] *Department of Electrical and Computer Engineering, National University of Singapore, 117 583, Singapore*
[d] *Laboratory of Technology and Solid Properties (LTPS), Abdelhamid Ibn Badis University of Mostaganem, 27000 Mostaganem, Algeria*
[e] *Research and Development Centre, Bharathiar University, Coimbatore 641 046, Tamil Nadu, India*
[f] *BPJ College of Arts and Science, Kozhai, Srimushnam, Cuddalore 608703, Tamil Nadu, India*
[g] *Chemistry Department, Faculty of Exact Sciences and Informatic, Hassiba Benbouali University, Chlef, 02000, Algeria*

ARTICLE INFO

ABSTRACT

The potential of 2,6-bis(4-fluorophenyl)-3,3-dimethylpiperidin-4-one (BFDP) as an anti-Parkinson's, anti-lung cancer, and anti-human infectious agent was extensively assessed in the current study. To accomplish this, the compound BFDP was synthesised and analysed using several spectroscopic approaches, such as NMR, mass and FT-IR spectral studies. The computational calculations for the molecule were carried out using density functional theory (DFT) at the B3LYP/6-311G++ (d,p) level of theory. A X-ray diffraction (XRD) study allows us to analyse the crystalline structure of our BFDP molecule. Intermolecular interactions were assessed using 3D Hirshfeld surfaces (3D-HS) and 2D fingerprint plots. AIM and NCI-RDG were done using quantum calculations and the DFT technique, and topological ELF and LOL, as well as vibrational parameters, have been obtained. The thermodynamic and thermal properties of the BFDP compound were determined. To investigate the pharmacokinetic characteristics of BFDP, a molecular docking study and an in silico ADMET study were done.

1. Introduction

The world's growing population, combined with radical changes in eating and living practices, is becoming one of the main causes

---

* Corresponding author.
** Corresponding author. Department of Chemistry, Karpagam Academy of Higher Education, Coimbatore 641 021, Tamil Nadu, India.
*** Corresponding author.
  E-mail addresses: thangabell2003@gmail.com (T. Arumugam), rarulraj108@gmail.com (A. Ramalingam), roufieda.guerroudj@yahoo.com (A.R. Guerroudj).

of illness in today's world, especially Parkinson's, human infectious diseases and lung cancer, represent the major sources of global invalidity, and are attracting greater attention [1,2]. Parkinson's illness affects the motor functions and communication of the patient, resulting in a deterioration of the nervous central body. The disease's clinical symptoms comprise muscular inflexibility, weakness and trembling of the body's movements [3]. Infectious diseases are caused by the penetration of one or several micro-organisms or infectious elements, including bacteria, fungi, parasites, protozoa and viruses, into tissue to multiply. Once the infectious agent is encountered by the target organism, the body's immune response is initiated [4]. On the other side, the World Health Organization has published some remarkable statistics in "World Cancer Report" by the International Agency for Research on Cancer, lung cancer results in 1.8 million deaths per year and remains the leading peak of cancer-related mortality [5,6].

Scientific researchers have pursued the development and synthesis of new organic compounds, with the aim of reducing this type of major disease worldwide. New organic piperidone compounds with excellent biological performance are being studied nowadays benefit from special interest owing largely over their ability to generate links [7–9]. This type of piperidone has essential synthetic qualities offering important medicinal, pharmacological and biological advantages, such as anti-Alzheimer's [10], insecticidal, fungicidal, anti-viral [11] and anti-tumor activity [12]. It has practical potential in the construction of photovoltaic panels, in non-linear optical processes, and in the advanced digital data storage and data transfer applications [13]. In this research context, our group was interested in synthesizing a new organic molecule from the piperidone family. The compound, 2,6-bis(4-fluorophenyl)-3, 3-dimethylpiperidin-4-one, BFDP ($C_{19}H_{19}F_2NO$), was analysed by X-ray diffraction and FT-IR spectroscopic techniques. The vibration modes have been measured according to a molecular structure optimization method derived from the B3LYP/6-311G++ (d,p) level. NLO effects have been developed to study the material's electronic and optical properties. The frontier molecular orbitals and the total electron density of the states were established to quantify the charge transfer within the BFDP structure. Topological analyses: electron localization function (ELF), localized orbital locator (LOL), reduced density gradient of non-covalent interactions (NCI-RDG), and atoms in molecules (AIM) were carried out. Hirshfeld surface analysis, 2D fingerprints interaction energies and energy frames offer valuable quantitative information about the contributions of each intermolecular interaction in the BFDP crystal. In addition, Global Chemical Reactivity Descriptors (GCRD), Molecular Electrostatic Potential (MEP), Fukui function, Mulliken and natural population describe the active sites and reactivity of the compound. Molecular docking and ADMET studies were performed to investigate its biological and pharmacokinetic activities.

Table 1
X-ray refinement parameters and crystal data for **BFDP.**

Compound	BFDP
CCDC	1557047
Chemical formula	$C_{19}H_{19}F_2NO$
Molecular weight (g.mol^{-1})	315.35
Temperature (K)	293(2)
Radiation wavelength(Å)	0.71073
Crystal System	monoclinic
Space group	P 2$_1$/n
a (Å)	12.1058(5)
b (Å)	7.1433(2)
c (Å)	18.8004(8)
α (°)	90
β(°)	93.5201(16)
γ(°)	90
Crystal size (mm)	$0.280 \times 0.260 \times 0.160$
V (Å^3)	1622.70(11)
Z	4
Density (g.cm^{-3})	1.291
μ (mm^{-1})	0.095
F(000)	664
Θ range for data correction(°)	1.95–27.38
h,k,l	$-15 \le h \le 15, -9 \le k \le 9, -23 \le L \le 24$
Number of measured, independent and observed[I > 2σ(I)] reflections	14801, 3671, 2538
Refinement method	full-matrix least-squares on F^2 data
Goodness of fit on F^2	1.005
R$_{int}$	0.021
Final R indices	
R_1	0.044
wR$_2$	0.121
R indices (all data)	
R_1	0.069
wR$_2$	0.141
Number of parametres	284

2. Experimental details

2.1. General

The melting point was determined using in open capillary method. The NMR spectra were acquired on a Bruker Avance III spectrometer running at 400.0 MHz (^{1}H NMR) and 100.0 MHz (^{13}C NMR) using TMS as a reference and CDCl$_3$ as the solution. FT-IR spectrum was recorded by NICOLET IS5 spectrometer using ATR mode. Agilent USA make 6470B was used for the determining triple quadruple LC-MS studies. To investigate the endo and exothermic phase transitions of BFDP, differential thermal analysis (DTA) and thermogravimetric analysis (TGA) were performed as well using the NETZSCH STA 2500 concurrent thermal analyzer.

### 2.2. Single-crystal X-Ray diffraction studies

A colorless crystal with a rectangular form and dimensions of $0.280 \times 0.260 \times 0.160$ mm^3 has been chosen to carry out an X-ray diffraction survey by means of a Bruker SMART-APEX-II single-crystal CCD diffractometer. X-ray data have been collected using MoK \a monochromatic graphite with a radiation of $\lambda = 0.71073$ Å. The program Shelxs was employed for solving the structure via direct methods [14]. This structure was refined by Shelxl [15]. Implementing in the WinGx software package [16], based upon a full least squares refinement algorithm. Anisotropic refinement of the non H atoms was applied. A single crystal of BFDP was formed by employing the slow evaporation solution via a technique utilizing ethanol as the solvent at ambient temperature. At the Cambridge Crystallographic Data Centre (CCDC 1557047), the crystalline structure of BFDP has been submitted. Hydrogen spaces bound to the C atoms were derived. The detailed results of the data analysis as well as the structure resolution are outlined in Table 1. The atomic positions and comparable isotropic movement parameters are reported in Table S1.

2.3. Computational details

The Density Functional Theory (DFT) method was highly effective for investigating the structural and chemical composition variations among different organic and mineral structures [17]. The 2,6-bis(4-fluorophenyl)-3,3-dimethylpiperidin-4-one computations have been carried out with the aid of the GAUSSIAN 09 molecular calculator and the Gauss-View molecular visualization package [18,19]. An X-ray parent structure was obtained from the X-ray data, and optimized by DFT with the Coulomb−attenuating (CAM−B3LYP) and the range−separated version of Becke's 97(WB97XD) utilizing the 6−311G++ (d,p) basis set. Potential energy distribution analysis software interprets the theoretical vibrations [20,21]. Moreover, the associated electonic molecular parameters featuring atom-in-molecule electron density analysis (AIM), reduced density gradient analysis of non-covalent interactions (NCI-RDG), localized orbital localization (LOL) and electron localization function (ELF) studies were calculated for the BFDP title compound at the same 6-311G++ (d,p) theoretical level. Additionally, the polarizability, dipole moment, and first-order hyperpolarizability were driven to determine nonlinear optical effects for the crystalline BFDP molecule. HOMO-LUMO, density of states, molecular electrostatic potential, global chemical reactivity descriptors, thermodynamic characteristics, Fukui function, Mulliken and natural population analysis were also simulated using the same DFT method. The 2D fingerprint plots with Hirshfeld surface analysis were performed on the single BFDP crystal using Crystal Explorer 17 software [22]. On the other hand, PASS and molecular docking, ADMET in silico were studied to investigate the theoretical biological activity of the BFDP component. The molecular docking was using by AutoDock Vina for docking and Discovery Studio Visualizer in order to visualize the ligand/protein receptor [23,24].

2.4. Synthesis of 2,6-bis(4-fluorophenyl)-3,3-dimethylpiperidin-4-one (BFDP)

BFDP was synthesised according to the protocol reported by Noller and Baliah [25] with minor changes. In short, an ethanol solution of ammonium acetate (0.05 mol, 50 ml) was mixed with *p*-flurobenzaldehyde (0.1 mol) and methyl isopropyl ketone (0.05 mol). The resultant reaction solution was reflexed for 10 min and left over-night at room temperature to obtain BFDP. The as-formed crude BFDP was separated, washed with ethanol and further purified by recrystallization in ethanol. The synthesis of BFDP is outlined in Scheme 1. The FT-IR, ^{1}H, ^{13}C NMR, and mass data on the BFDP compound are reviewed in depth in the result and discussion
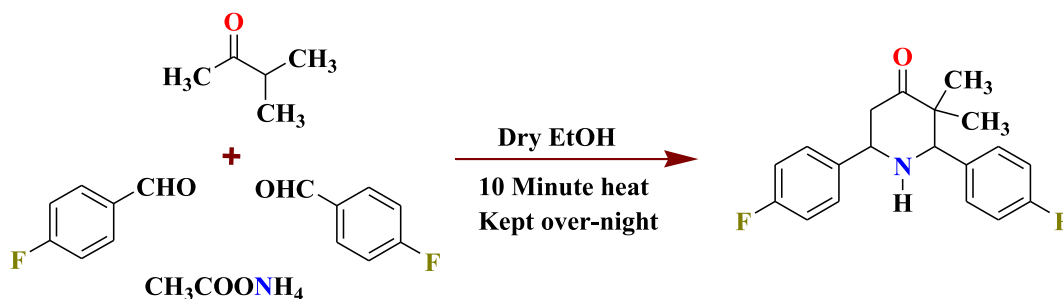
Scheme 1. Synthetic scheme of 2,6-bis(4-fluorophenyl)-3,3-dimethylpiperidin-4-one.

sections.

3. Results and discussion

3.1. Spectral studies

3.1.1. FT-IR spectral studies

In the position of 2,6 substituted piperidin-4-one compounds, a chair conformation is often identified [26–28], however, the conformation can change according to the substitution in the phenyl ring [29–32]. The FT-IR spectrum of BFDP (Fig. 1) shows N–H stretching and C–H (aromatic) stretching at 3307 and 3050 cm^{-1}, respectively. The aliphatic C–H stretching vibration was noted at 2964 and 2930 cm^{-1}. A sharp band present at 1696 cm^{-1} can be assigned to C=O group of BFDP. The lone pair of electrons present on nitrogen atom in a stable piperidine conformation is likely to be in the axial position. Such conformation can be analysed by Bohlmann band [33]. Generally, 2,6-disubstitued piperidones showed Bohlmann bands in the range of 2850-2700 cm^{-1}. In Fig. 1, a Bohlmann band is appeared at 2823 cm^{-1}, indicating the presence of anti-periplanar axial hydrogen atom at the two alpha sites in piperidine ring. This result infers that the piperidine unit in BFDP is in a chair conformation (Fig. S4). The IR spectral frequencies of BFDP were presented in Table S2.

3.1.2. NMR and mass spectral studies

In the ^{1}H NMR spectrum (Fig. S1), two singlets with six protons are observed at 0.96 and 1.20 ppm which corresponds to two methyl groups (C-3 carbon). The broad peak appeared at 1.95 ppm can be assigned to N–H group [34]. The benzylic protons exist at C-2 and C-6 are resonated as singlet and doublet of doublet at 3.83 ppm and 4.06 ppm (J = 12.0 & 2.8 Hz), respectively. The axial and equatorial methylene proton (H$_b$) at C-5 is appeared as doublet of doublet at 2.89 ppm (J = 13.6 & 12.0 Hz) and 2.46 ppm (J = 13.8 & 3.0 Hz), respectively. The multipets in the region of 7.04–7.51 ppm are due to the aromatic ring protons at C-2 and C-6. The presence of one huge (12.0 Hz) and small coupling (2.8 Hz) about J$_{H(5),\ H(6)}$ bond in piperidin-4-one of BFDP reveals that this compound adopt normal chair conformation with equatorial orientation of aryl rings at C(2) and C(6) and methyl groups at C(3). In the ^{13}C NMR spectrum (Fig. S2), a peak at 19.91 and 20.40 ppm is due to methyl groups (C-3), whereas, C-5 and C-3 carbons showed peaks at 47.33 and 49.82 ppm, respectively. The benzylic carbons (C-2 and C-6) showed characteristic peak at 68.81 and 60.94 ppm and the peaks in the region of 114.74–162.42 ppm are owing to the aromatic carbons. The peak ascribed to carbonyl carbon (C-4) is appeared at 212.17 ppm. The structure of BFDP can be confirmed by LC-MS spectrum analysis (Fig. S3). The peak at 316.2 *m/z* confirms the presence of compound BFDP structure.

3.2. Molecular geometry

The BFDP's optimized structure has been calculated using the two functionals CAM−B3LYP and WB97XD based on the 6−311G++ (d,p) level. These computations have been carried out using an isolated molecule in gaseous deposition [35]. The BFDP structure with the atomic numbering pattern following the [110] miller indices position was given throughout Fig. 2. The simulated and experimental BFDP compound geometries are listed in Table S3. The C−C bond length median was estimated to be ≈ 1.424 Å experimental reading, 1.528 Å employing the DFT/CAM−B3LYP method and 1.322 Å via the WB97XD approach using the same 6−311G++(d,p) basis set. The bond angles range from 106.16 to 122.77° values in terms of the experimental findings. While, the optimized angles are between [106.98°–122.26°] by utilizing the CAM−B3LYP functional methods and in the range of [106.52–122.19] by using the WB97XD
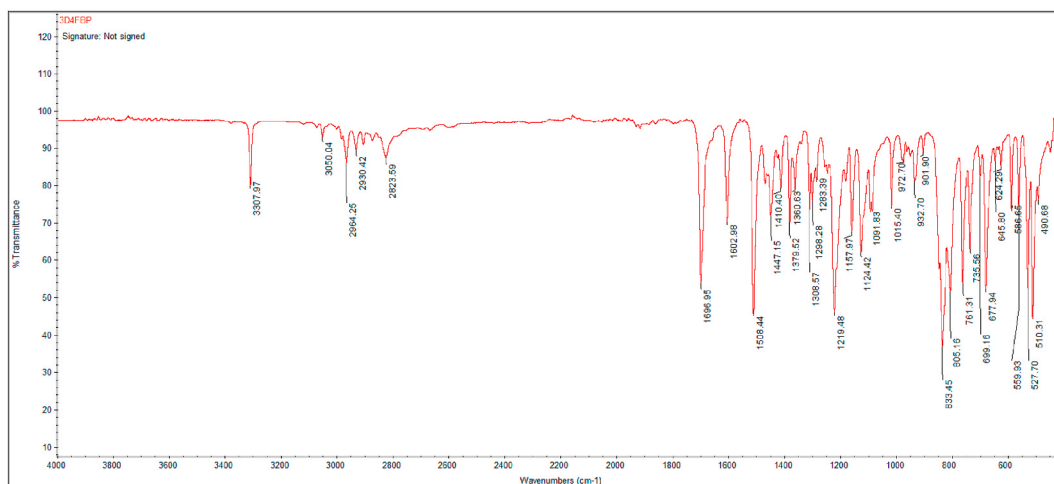

Fig. 1. FT-IR spectrum of 2,6-bis(4-fluorophenyl)-3,3-dimethylpiperidin-4-one.
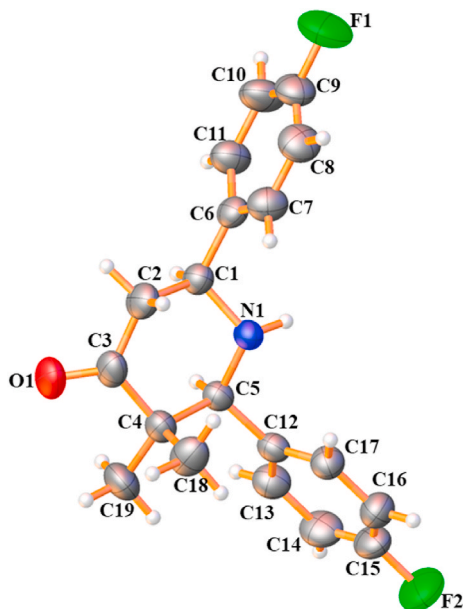
Fig. 2. Overview with the atomic numbering pattern of the BFDP compound.

feature. Accordingly, the dihedral angles have a divergence of at most 1.57° for the N1−C1−C6−C7 predicted by means of WB97XD and 0.61° with the use of B3LYP/6−311G++ (d,p) basis set. Therefore, CAM−B3LYP was more reliable than WB97XD compared with the findings of XRD data. The resulting geometrical settings on all theoretical dimensions proved to be in accordance to crystallographic data. The crystal packaging graphical diagram and interactions of hydrogen links are illustrated in Fig. S5 and Fig. S6 respectively. According to Table 2, the BFDP molecule consists of numerous H−bonding interactions. In the BFDP molecule, the C−H⋯O hydrogen bonding intermolecular distance equals 2.51 Å and the C−H⋯F hydrogen bonding intermolecular distance equals 2.53 Å and 2.60 Å with F2 and F1 atoms.

3.3. Hirshfeld surface analysis and 2D fingerprint plots

The calculation of Hirshfeld surfaces has evolved into a useful tool for crystallographers and crystal engineers since it gives additional insight into weak intermolecular forces [36]. A Hirshfeld surface was defined by the density weighting factor of the particular molecule of interest over the same sum of the density of its nearest neighbor, resulting in an isosurface with 0.5 arbitrary units. Different things, like electrostatic potential, d_{norm}, curvedness, and shape-index can be mapped onto Hirshfeld surfaces. These are valuable for gathering more data on weak intermolecular interactions. Crystal Explorer 17 may be obtained at http://crystalexplorer.scb.uwa.edu.au/downloads.html (Turner et al., 2017). The Hirshfeld surfaces plotted over d_{norm} use the function of normalized distances d_e and d_i, where de and d_i are the distances from an actual surface spot to the nearest atom just on the surface's outside as well as inside, in both. The white, red and blue color schemes being used on d_{norm}-mapped Hirshfeld surfaces identify longer interatomic interactions, van der Waals isolation, and shorter interatomic contact information, respectively [37,38].

With the help of Crystal Explorer 17.5, HS (Hirshfeld surfaces) were made to show how the BFDP molecule interacts with its crystal structure. In this surface study, the value ranges from 0.9450 to 2.6217, representing the distance between the surface point and the nucleus closest to the surface. Fig. 3 shows the Hirshfeld analysis for the BFDP using the d_{norm} and a molecule next to it that is above the surface. The red zone depicts the interaction between oxygen (O) and hydrogen (H) atoms that is most significant. Fig. 4 depicts the Hirshfeld surfaces for d_e, d_i, d_{norm}, curvedness, and shape index of the BFDP molecule. The normalized distance of the BFDP structure's larger contact d_{norm} value ranges between −0.2946 and 1.4629. The red region on the outermost layer depicts the interatomic contacts engaged in strong hydrogen bonding and inter-atomic connections. Fig. 5(a-h) presented the 2D fingerprint plots of the primary intermolecular interactions and fraction of different intermolecular interactions that made up to the Hirshfeld surfaces, (a) H⋯H (50.4 %); (b) H⋯F/F⋯H (20.0 %); (c) C⋯H/H⋯C (14.3 %); (d) H⋯O/O⋯H (8.7 %); (e) C⋯C (2.4 %); (f) C⋯F/F⋯C (1.6 %); (g) F⋯F (1.6

Table 2
Intermolecular interaction geometries for BFDP structural analysis.

D−H⋯A	D−H (Å)	D−A (Å)	H⋯A (Å)	D−H⋯A (°)	Equivalent positions
C13−H13⋯F1	0.95 (17)	3.47 (2)	2.60(17)	151.5(13)	-x+1,-y+1,-z
C16−H16⋯F2	0.92 (19)	3.44(2)	2.53(2)	173.0(16)	-x+1,-y+1,-z+1
C17−H17⋯O1	0.98 (17)	3.42(2)	2.51(17)	154.8(13)	-x+1/2,+y-1/2,-z+1/2
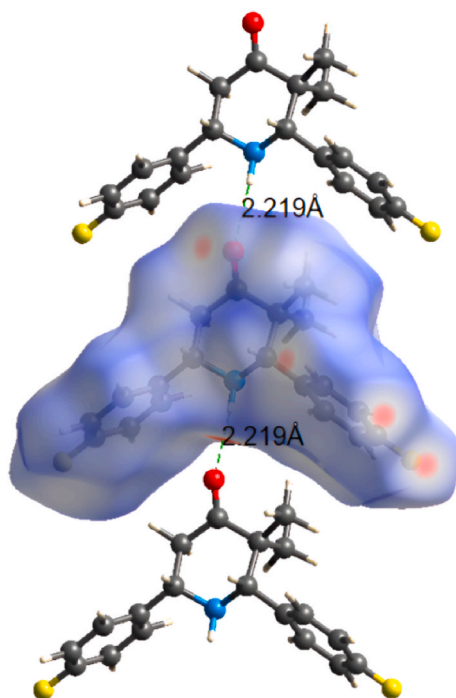
Fig. 3. Hirshfeld analysis plotted with d_{norm} shows neighboring molecules outside of the surface for the BFDP.
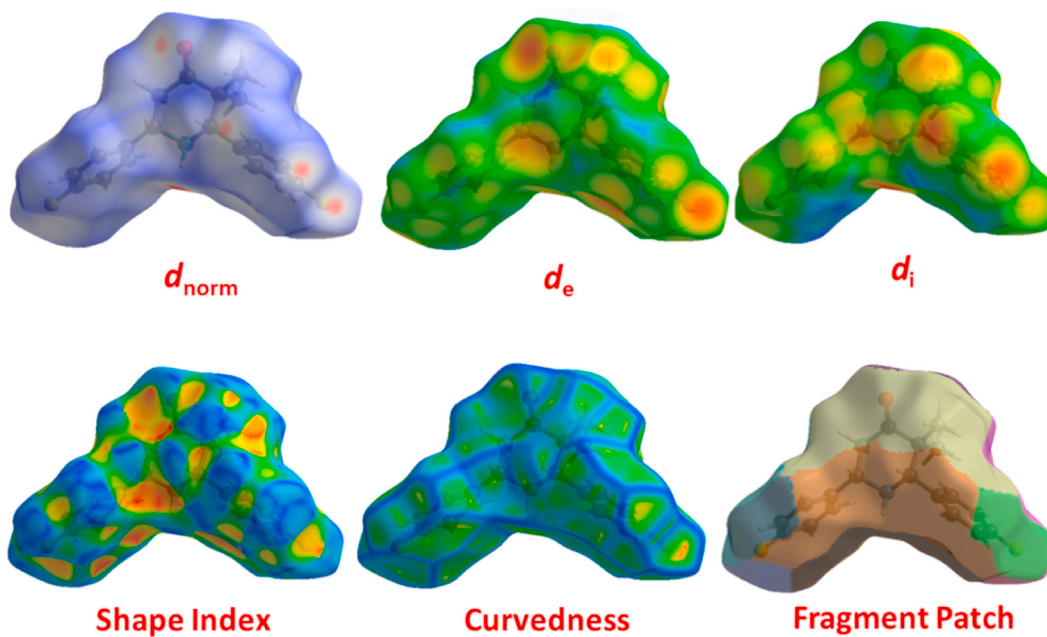
Fig. 4. Some Hirshfeld surfaces for the BFDP.

%); (h) O⋯C/C⋯O (0.7 %) in the BFDP compound.

3.4. Atom in molecule of electronic density (AIM)

Atoms in molecules (AIM) represents a quantum chemical framework that describes the chemical topology of the electron density of the system under study which determines the spatial allocation of the electrons [39,40]. The use of an AIM method provides a deeper
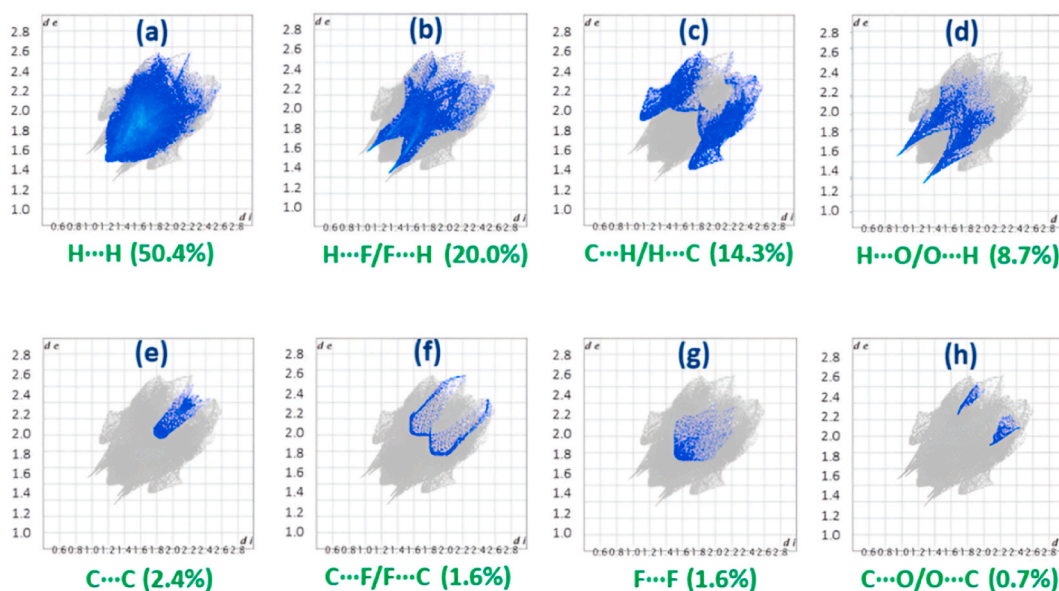
Fig. 5. 2D Fingerprint plots of Hirshfeld surfaces for BFDP (a) H⋯H (50.4 %); (b) H⋯F/F⋯H (20.0 %); (c) C⋯H/H⋯C (14.3 %); (d) H⋯O/O⋯H (8.7 %); (e) C⋯C (2.4 %); (f) C⋯F/F⋯C (1.6 %); (g) F⋯F (1.6 %); (h) O⋯C/C⋯O (0.7 %).

comprehension of non-covalent chemical reactions revealed inside a molecular structure as well as a detailed description of the hydrogen bonds' properties according to the different energetic and topological parameters available in the molecular structure. Some of these characteristics include: the eigenvalues of the hessian matrix (λ1, λ2, λ3), Potential energy density V(r), Hamiltonian Kinetic Energy H(r), Lagrangian Kinetic Energy G(r), Laplacian of electron density $\nabla^2\rho(r)$ and Electron density (ρCP). This method locates the critical density points corresponding to a topological character. The optimized BFDP molecule has been employed in order to compute the different characteristics by the use of Multiwfn software [41]. Our investigated molecule has three ring critical (RCPs) on 50, 61, 77 points and non-bond critical point (Fig. S7). The point of zero gradient ($\nabla\rho = 0$) of the electron density is considered to be the critical point according to Bader's theory. The total of the three eigenvalues of the Hessian matrix (λ1, λ2, λ3) fits the Laplacian of the electron density. The ring critical of three point 50, 61 and 77 are moderate for reason of its Laplacian of the electron density $\nabla^2\rho(r)$ and potential energy density V(r) for the BFDP compound. The different topology ring critical points parameters of BFDP crystal compound are listed in Table 3 The electron density (ρRCP) is equal to 0.222912, 0.022298 au for the both aromatic ring critical points 50 and 66 and 0.019040 for RCP-77. The Lagrangian Kinetic Energy G(r) was 0.033181, 0.033181 and 0.024183 au for the three RCPs. Also, the Hamiltonian Kinetic Energy H(r) present a negativevalues of −0.007455, −0.007469, −0.005691 au for RCP-50, RCP-61 and RCP-77 respectively.

3.5. Non covalent interactions reduced density gradient (NCI-RDG) analysis

The non-covalent reduced gradient NCI-RDG density technique was applied to investigate the various non-covalent chemical interactions existing inside the compounds [42]. The NCI-RD is based on the 0.5 isosurface value. The fondamental reduced density gradient (RDG) consists to quantify is the density and its first derivative as bellow [43] (Equation (1)):

$$\text{RDG(r)} = \frac{1}{2(3\pi^2)^{\frac{1}{3}}} \frac{|\nabla\rho(r)|}{\rho(r)^{\frac{4}{3}}} \tag{1}$$

The range of the various interactions are illustrated by bleue, green and red colorsbtween −0.035 to 0.02 atomic unit. The repulsive

Table 3
Topological parameters of hydrogen bonded interaction for BFDP molecule.

Parameters (a.u)	RCP-50	RCP-61	RCP-77
Electron density (ρRCP)	0.222912	0.022298	0.019040
Laplacian of electron density $\nabla^2\rho(r)$	0.162548	0.162601	0.119496
Lagrangian Kinetic Energy G(r)	0.033181	0.033181	0.024183
Hamiltonian Kinetic Energy H(r)	−0.007455	−0.007469	−0.005691
Potential energy density V(r)	−0.025725	−0.025711	−0.018492
Eigen Value λ1	0.085680	0.086383	0.062509
Eigen Value λ2	−0.016798	−0.016856	0.071802
Eigen Value λ3	−0.016798	0.093074	−0.014815

interactions are dashed in red (steric effect). The strongest steric repulsive influences usually related to π-π packing interactions across the molecule that have been seen in the centers of the three rings of the molecule. The green and red color area surrounding (C11, H11) of the aromatic ring and (N1, H1) of the piperidine ring accounting for a steric area. While the green areas depict the Van der waals binding reactions which are potentially implicated for stability of the BFDP compound molecular system. Fig. 6 (A) depicts the scatter diagram and Fig. 6 (B) the gradient isosurfaces for BFDP molecule.

3.6. ELF and LOL studies

The localized orbital locator (LOL) and electron localization function (ELF) are valuable covalent linkage assay tools indicating locations of the high probability of electron pairs in the molecule [44]. ELF was developed by Edgecombe and Becke. Both are based on the electron kinetic energy density [45]. Confirming the need for ELF computation by methods based on density functional theory. The numbers of η(r) are usually found to be in the range of 0–1.0. Large values in the range 0.5 and 1.0 correspond to domains consisting of localized non-bonding and bonding electrons, while smaller measurements (<0.5) denote regions where electrons must be delocalized. The LOL series of measurements (0–1.0) is similar to the ELF series of measurements meaning that chemical content equality. Therefore, the LOL provides a clearer and more decisive view than the ELF. Covalent bond surface analysis was performed to investigate ELF and LOL techniques. From LOL mapping, the electron beam has been displaced towards certain carbon atoms especially C9, C3, C15 and C19 atoms in our studied molecule, which is marked by blue shading Fig. 7(A) and (B) display the shaded surface map with projection impact of the localized orbital locator (LOL) map and electron localization function (ELF) of the BFDP. The critical points, their plots and their chemical relevant bounds are clearly visible on the ELF map. These are located in the high density zones around the hydrogen atoms found within the molecule. The central regions of some hydrogen atoms are highlighted in white, indicating that the electron density exceeded the maximum limit of the chromatic scale 0.80 (LOL mapping Fig. 7(B)).

3.7. Molecular electrostatic potential analysis

The molecular electrostatic potential is an effective device for determining electron density [46,47]. The electron density distribution and is relevant for the electrophilic reactions and nucleophilic attacks and more importantly hydrogen bonding interactions. The MEP was derived by applying the hybrid functional B3LYP with the $6-311G++(d,p)$ level in order to provide information on intermolecular reaction areas [48]. The molecular electrostatic potential was defined using the following indicated equation (2):

$$V(r) = \sum_A \left(\frac{Z_A}{|R_A - r|} - \int \frac{\rho(r)dr'}{r' - r} \right) \tag{2}$$

In which Z_A denotes the charge of the nucleus A located in R_A and $\rho(r)$ present the electrical density. A range of different representative colors i.e., red, orange, yellow, green, and blue have been illustrated in the MEP pattern to reflect the electrostatic potential locations. Fig. 8(A) and (B) shows that the oxygen atom O1 has the most negative electrostatic potential with -4.86 e^{-2} denoted by red and the
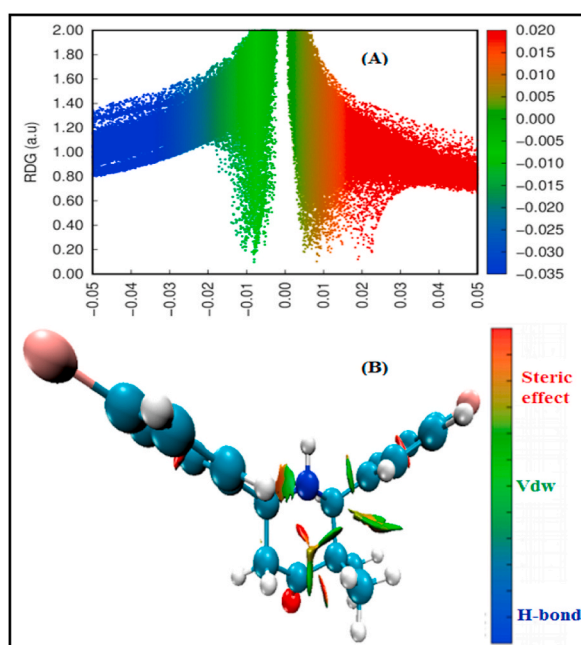
Fig. 6. (A)The scattering diagram and (B) gradient isosurfaces for BFDP.
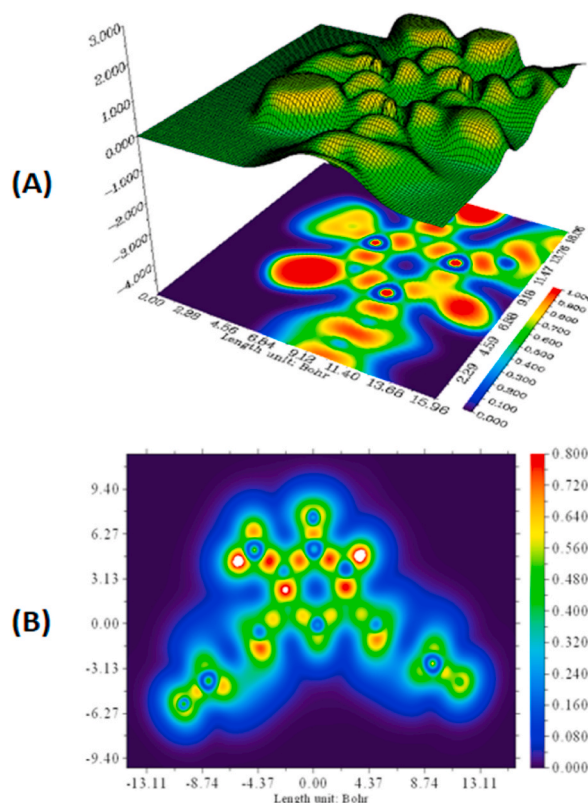
Fig. 7. (A) Covered surface map with projection impact of the electron localization function (ELF); (B) Localized orbital locator (LOL) pattern of the CFDP.
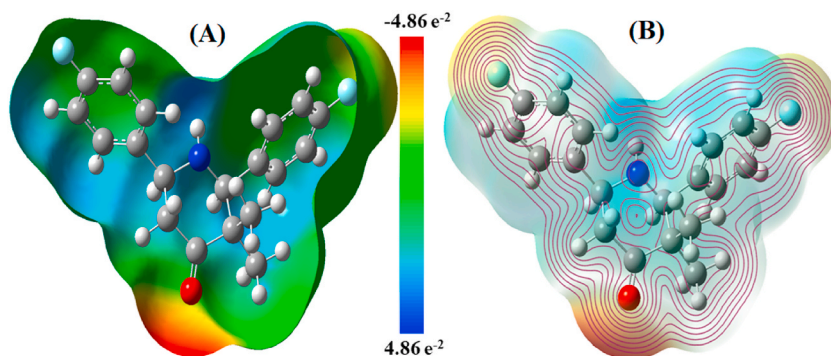
Fig. 8. (A) Total electron density surface solid mapping and (B) contour mapping ofmolecular electrostatic potential (MEP) for BFDP molecule.

two fluorine atoms F1 and F2 in yellow color indicating the electrophilic potential zones. On the contrary, the blue color corresponds to the nucleophilic site which is situated at the hydrogen areas in the whole organic compound.

3.8. Vibrational band assignments

The use of vibration spectroscopy is widely practiced in the field of organic chemistry to identify the individual functional groups present in the material [49,50]. It has been performed to verify that experimental vibrational spectra such as the theoretical vibration analysis. The molecule is made of 42 atoms that exhibit 95 fundamental normal vibration modes. In our research, the calculated frequencies were determined by using the B3LYP and WB97XD functionals in gas-phase using $6-311++G$ (d, p) level. The different frequencies assignments are collected on the basis of the potential energy distribution (PED) that has been performed with the VEDA 4 software [51]. In general, the measured oscillation wavenumbers are significantly higher in relation to the measured values of the observed data. Therefore, the calculated systematic wavenumber errors were minimized with a scaling factor of 0.967 for both

Table 4

Comparison of the calculated harmonic frequencies using the B3LYP/6311G++(d, p) technique and experimental FT-IR wavenumbers (cm^{-1}) for BFDP.

No	Experimental FT-IR	CAM−B3LYP		WB97XD		Assignments with PED>10 %
		Scaled	I_R	Scaled	I_R	
95	3459.73	3446.74	2.6106	3450.39	1.8829	ν NH (100)
94	3127.80	3123.89	0.9097	3128.21	2.4237	ν CH (92)
93		3117.95	1.8421	3127.21	2.7936	ν CH (86)+ ν CH$_{asy}$ (14)
92		3117.44	1.2724	3124.62	2.3450	ν CH (51)+ ν CH$_{asy}$ (45)
91		3117.32	0.7946	3122.55	2.2896	ν CH (48)+ ν CH$_{asy}$ (43)
90		3108.51	2.1342	3112.38	2.3827	ν CH (46)+ ν CH$_{asy}$ (47)
89		3101.01	2.4653	3105.33	3.5477	ν CH (86)
88		3089.31	4.8074	3095.60	6.0773	ν CH (89)+ ν CH$_{asy}$ (47)
87		3084.74	5.1543	3090.71	6.5624	ν CH (38)+ ν CH$_{asy}$ (62)
86		3044.43	16.1104	3047.28	12.0875	ν CH (50)+ ν CH$_{asy}$ (46)
85		3043.46	12.3735	3045.96	18.8540	ν CH (54)+ ν CH$_{asy}$ (39)
84		3036.31	12.2702	3042.56	15.5084	ν CH (11)+ ν CH$_{asy}$ (69)
83		3029.19	17.6448	3028.70	21.7378	ν CH (21)+ ν CH$_{asy}$ (68)
82		3023.13	13.3173	3027.16	13.6093	ν CH (10)+ ν CH$_{asy}$ (81)
81		2970.17	6.0216	2970.56	7.0038	ν CH (81)
80	2965.50	2964.02	13.6889	2957.39	14.8277	ν CH (81)
79		2959.02	13.4388	2954.88	18.8927	ν CH (44)+ ν CH$_{asy}$ (36)
78		2852.07	39.3763	2846.05	36.4095	ν CH (24)+ ν CH$_{asy}$ (73)
77	2824.72	2845.99	41.4629	2839.27	53.3558	ν CH (50)+ ν CH$_{asy}$ (48)
76	1749.05	1758.35	246.0499	1762.85	252.8999	ν OC (93)
75	1625.60	1621.63	28.9309	1621.87	30.2504	ν CC (43)
74	1503.04	1517.32	3.0415	1500.08	3.0870	ν CC (49)+ δ CCC$_{asy}$ (10)
73		1513.29	89.1471	1510.21	97.9440	δ HCC$_{asy}$ (23)+ δ HCC (23)
72	1509.03	1511.82	162.1247	1508.48	154.2730	δ HCC (44)
71		1474.01	28.8280	1477.77	19.0381	δ HCH (65)+ τ HCCC$_{asy}$ (10)
70		1461.73	15.6362	1464.54	22.1788	δ HCH (51)+ δ HCH$_{asy}$ (17)+ τ HCCC$_{asy}$ (10)
69	1448.28	1448.03	12.0229	1447.88	5.3247	δ HCH$_{asy}$ (51)+ τ HCCC$_{asy}$ (13)
68		1446.30	32.9033	1444.43	55.4999	δ HNC (35)+ δ HCH$_{asy}$ (12)
67		1443.47	38.5758	1440.27	29.0440	δ HNC$_{asy}$ (17)+ δ HCH$_{asy}$ (41) + τ HCCC (12)
66		1425.86	7.2974	1426.74	22.4060	δ HCH$_{asy}$(48)+ δ HCH(14)
65		1421.45	12.1943	1420.36	1.3242	δ HCN (12)
64		1417.59	3.2648	1414.74	2.6599	δ HCC$_{asy}$ (13)
63		1383.72	29.2136	1378.06	25.9759	δ HCH(84)
62	1379.81	1370.52	12.1746	1366.83	11.6292	δ HCN(40)
61		1362.17	9.9109	1357.74	7.5991	δ HCH (32)+ δ HCH$_{asy}$ (29)
60		1344.74	11.3721	1339.15	19.4712	δ HCN (25)
59		1340.00	16.4930	1333.21	11.9989	δ HCN(23)+ τ HCCC$_{asy}$ (14)
58	1308.94	1308.16	61.6489	1300.63	59.8075	ν NC (11)+ τ HCCC$_{asy}$ (17)
57		1289.25	16.1746	1290.54	19.9138	ν CC (23)
56		1285.79	18.1374	1285.38	8.9241	δ HCC(63)
55		1281.59	1.6608	1284.31	4.1265	δ HCC(18)+ δ HCC$_{asy}$(17)
54		1276.18	12.0859	1279.74	18.0879	ν CC (10)
53		1256.31	6.4821	1251.62	7.2660	τ HCCC$_{asy}$ (20)
52		1247.69	2.8692	1245.71	2.9221	δ HCN(19)
51		1228.35	71.9281	1227.84	76.2261	ν CC$_{asy}$ (22)+ ν FC (41)
50	1219.75	1226.96	173.3854	1226.18	170.5315	ν CC$_{asy}$ (11)+ ν FC (32)+ ν FC$_{asy}$ (13)
49		1204.74	15.8857	1202.70	14.4975	ν CC$_{asy}$ (16)
48		1198.75	5.3724	1196.04	4.4469	ν CC$_{asy}$ (11)+ δ HCN(13)
47		1189.36	9.9816	1187.00	9.9628	ν CC$_{asy}$ (12)+ δ HCC(10)
46		1177.41	24.5390	1175.43	17.8299	δ HCC(26)+ τ HCCC$_{asy}$ (12)
45		1157.93	2.3371	1155.14	9.9953	δ HCC$_{asy}$(22)
44		1147.24	19.0437	1152.28	6.0953	δ HCC(34)
43		1145.45	9.5128	1149.78	19.4295	δ HCH$_{asy}$(10)+ δ HCC$_{asy}$(22)
42	1124.77	1137.11	80.3963	1144.32	80.2783	ν NC$_{asy}$ (38)
41	1116.30	1107.97	12.5095	1109.26	5.8379	δ HCC$_{asy}$(18)
40		1101.16	7.6941	1090.79	6.2607	δ HCC(33)+ δ HCC$_{asy}$(15)
39		1086.46	5.4095	1081.85	17.3489	δ HCC(21)
38		1079.33	15.6541	1005.11	15.5633	δ CCC$_{asy}$(18)
37		1009.27	6.3571	1004.98	4.6775	ν CC$_{asy}$ (12)+ δ CCC(14)+ δ CCC$_{asy}$ (18)
36		1008.81	14.1751	1002.64	1.3770	τ HCCC (11)
35		1006.64	0.7586	975.44	1.4552	τ HCCC (34)+ τ HCCC$_{asy}$ (35)+ τ CCCC (14)
34		979.31	1.2564	973.12	2.5618	τ HCCC$_{asy}$ (33)
33		975.39	4.7801	969.57	5.8369	τ HCCC (37)
32		971.36	3.7328	957.46	1.2045	τ HCCC (36)+ τ HCCC$_{asy}$ (13)
31		959.17	0.8826	947.02	0.5593	τ HCCC$_{asy}$ (70)
30		949.95	1.0201	945.70	4.7394	τ HCCC$_{asy}$ (30)

(continued on next page)

Table 4 (*continued*)

No	Experimental FT-IR	CAM−B3LYP		WB97XD		Assignements with PED>10 %
		Scaled	I_R	Scaled	I_R	
29		943.36	4.4038	931.71	1.6518	ν CH$_{asy}$ (15)+ τ HCCC (10)+ τ HCCC$_{asy}$ (29)
28	927.96	935.60	1.7656	924.10	6.5215	ν CC (11)
27		924.95	6.7861	901.76	2.5057	ν CC$_{asy}$ (10)
26		900.93	2.7488	852.10	34.5014	τ HCCC$_{asy}$ (34)
25		853.13	29.8743	844.35	74.6459	τ HCCC$_{asy}$ (69)+γFCCC(12)
24		846.65	75.8848	827.85	20.5266	τ HCCC$_{asy}$ (10)+ τ HCCC (11)
23		845.30	15.3947	825.38	5.8825	τ HCCC$_{asy}$ (35)+ τ HCCC (20)
22	834.54	829.58	23.2817	822.46	4.7285	τ HCCC (75)
21		823.78	2.1774	801.39	25.4355	ν CC$_{asy}$ (11)+ ν FC$_{asy}$ (30)+ ν CC (11)
20		820.97	1.5747	792.59	11.0451	δ CCC$_{asy}$(12)+ τ HNCC$_{asy}$ (12)
19		803.12	25.4744	752.91	20.3432	τ HNCC$_{asy}$ (10)
18		792.80	11.8060	734.44	9.0308	τ CCCC$_{asy}$ (32)
17	762.22	753.65	20.4962	726.32	2.3603	τ CCCC$_{asy}$ (11)+ τ CCCC (38)
16		737.02	7.3581	697.96	9.2099	ν CC (38)+ γ OCCC$_{asy}$(11)
15		729.54	3.3012	670.63	33.7888	τ HNCC$_{asy}$ (18)+ γ OCCC(18)
14	677.89	698.44	9.0626	637.76	1.4166	δ CCC$_{asy}$(20)+ δ CCC (10)
13	674.48	669.78	34.6304	628.85	0.8963	δ CCC (34)
12		639.66	1.1168	617.13	2.4636	δ CCC (19)
11	587.70	632.78	0.7290	585.73	2.5426	δ CCN$_{asy}$ (34)+ δ OCC$_{asy}$ (34)
10		619.02	2.8357	525.21	15.1096	γ FCCC$_{asy}$(17)
09		585.69	2.3481	512.20	21.3018	δ OCC (16)+ τ CCCN$_{asy}$ (15)+ γ FCCC(19)
08		553.58	11.8171	489.64	0.7736	δ CCC (10)
07		534.93	30.8514	440.19	0.2438	γ CNCC$_{asy}$(10)
06		523.44	17.5105	420.78	0.1477	τ HCCC$_{asy}$ (10)+ τ CCCC (69)
05		509.38	16.7920	417.09	0.0548	τ HCCC (21)+ τ CCCN$_{asy}$ (44)+ τ CCCC (11)
04		488.90	0.6377	414.79	6.3321	δ FCC (26)+ τ CCCC$_{asy}$ (12)+ γ FCCC$_{asy}$(11)
03		437.33	0.2412	411.49	4.6794	δ FCC (38)+ δ FCC$_{asy}$ (10)
02		422.71	0.1201	406.20	0.3732	δ FCC$_{asy}$ (46)
01		419.74	0.1649	379.81	2.9501	τ CCCC$_{asy}$ (26)+ γ FCCC$_{asy}$(21)

asy: asymmetric; ν: stretching; γ: out of plane bending; δ: bending; τ: torsion.

CAM−B3LYP and WB97XD for the title component employing the same 6−311G++(d,p) basis set. The comparison of FT−IR and calculated IR spectra for BFDP was shown in Fig. S8. The comparison of the estimated harmonic frequencies utilizing the B3LYP/6311G++(d, p) technique and experimental FT−IR wavenumbers (cm^{-1}) for BFDP was provided in Table 4. The vibrational modes were determined by the potential energy distribution (PED). The scaled frequencies are in units of cm^{-1}.

The vibrational bands of C–H stretching are typically seen in the interval 3100-3000 cm^{-1}. In our molecule, the ν (CH) has been observed from 2845.99 cm^{-1} to 3123.89 cm^{-1} using CAM−B3LYP functional, from 2839.27 cm^{-1} to 3128.21 cm^{-1} by WB97XD and at 3127.80, 2965.50, 2824.72 cm^{-1} for experimental ν (CH) frequencies. For our crystalline compound, the carbonyl stretching vibrations were observed at 1749.05 cm^{-1} in the experimental FT−IR spectrum, and at 1758.35, 1762.85 cm^{-1} calculated by the CAM−B3LYP and WB97XD functionals respectively with 93 % PEDs. The stretching vibrations of C=C band usually are situated in the area 1600-1400 cm^{-1}. In our research, the experimental ν (C=C) occurs at 1625.60, 1503.04 cm^{-1} experimentally, at 1621.63, 1517.32 cm^{-1} for CAM−B3LYP and 1621.87, 1500.08 cm^{-1} for WB97XD. The computed stretching vibration for ν (N–H) observed at 3446.74, 3450.39 cm^{-1} for both CAM−B3LYP and WB97XD simulated functionals and 3459.73 cm^{-1} empirically with a PEDs level of 100 %. The symmetrical ν (NC) assignments were observed at 1308.94 cm^{-1} in the FT−IR spectrum and at 1308.16, 1300.63 cm^{-1} in the theoretical spectra. While the asymmetrical ν$_{asy}$ (NC) frequency has been depicted at 1137.11, 1144.32 cm^{-1} in the CAM−B3LYP and WB97XD spectrums with 1124.77 cm^{-1} experimental bond of vibration. The asymmetrical out of plane FCCC band vibrations were occurred at 619.02, 419.74 cm^{-1} for the CAM−B3LYP functional readings and 525.21, 379.81 cm^{-1} wavenumbers.

3.9. Frontier molecular orbitals (FMOs) and total electronic density of states

The molecular orbitals and their characteristics, especially in terms of energy are used to predict the most likely type of several reactions for the molecule [52]. The lowest occupied molecular orbitals (LUMO) and most occupied molecular orbitals (HOMO) the represent the major molecular orbital boundaries in a given molecule [53,54]. The HOMO energy was closely associated with the ionization potential with energy of −8.50 eV. While, the lowest occupied molecular orbitals (LUMO) energy was mainly dependent on the electron affinity that has energy of 0.13 eV. The energy gap between HOMO-LUMO is equal to 8.37 eV (Fig. S9(A)). The π electron was delocalized especially on the C−C bond through the two aromatic rings of the molecule. The HOMO is localized in the whole molecule except for the two methyl of the piperidine ring and the LUMO is especially situated on one of the aromatic ring indicating the charge transfer inside the molecule. However, owing to the charge transfer inside the molecule through the HOMO and LUMO orbitals, the π−π* type transitions were seen. Fig. S9(B) presents the density of state (DOS) of the BFDP compound. The green lines belong to the occupied molecular orbitals. Red created the unoccupied molecular orbitals. The investigation of the DOS indicates that the gap energy band is achieved at roughly 8.37 eV for the level of theory CAM−B3LYP/6−311G++(d,p).

3.10. Global chemical reactivity descriptors (GCRD)

Chemical reactivity and molecular structure have a significant correlation with global chemical reactivity descriptor (GCRD) parameters such as Chemical hardness (η) (Equation (3)), Electronegativity (χ) (Equation (4)), Electron affinity (A) (Equation (5)), Chemical softness (s) (Equation (6)), Electrophilicity index (ω) (Equation (7)), Ionization potential (I) (Equation (8)), Dipole Moment (μ) (Equation (9)) and Hyper-hardness (Γ) (Equation (10)). These parameters can be derived from the following equations:

$$\eta = 1/2 \left(E_{LUMO} - E_{HOMO}\right) \tag{3}$$

$$\chi = -\frac{1}{2}\left(E_{LUMO} + E_{HOMO}\right) \tag{4}$$

$$A = -E_{LUMO} \tag{5}$$

$$S = 1/2\,\eta \tag{6}$$

$$\omega = \frac{\mu^2}{2\eta} \tag{7}$$

$$I = -E_{HOMO} \tag{8}$$

$$\mu = 1/2\left(E_{LUMO} + E_{HOMO}\right) \tag{9}$$

$$\Gamma = E_{LUMO} - 2E_{HOMO} + E_{HOMO-1} \tag{10}$$

The calculated global chemical reactivity descriptors have been collected in Table 5. The BFDP compound shows −1064.90 atomic unit of energy. The value of 4.32 eV of the chemical hardness (η) compared to the chemical softness (s) which has 2.16 eV indicates that the title molecule has a hard structure confirmed by the high mesurment of Hyper-hardness (Γ) parameter. The molecular structure has a low electrophilic behaviour with 0.14 eV of electrophilicity index (ω). The BFDP is stable molecule by its −4.32 eV of Chemical potential (P) reading.

3.11. Fukui function, mulliken and natural population analysis

The prediction of the several aspects of the reactive mechanism available, and the localization of the electrophilic, nucleophilic or radical character zones of reactivity in the studied formula, local quantifications as the Fukui functions, Mulliken charges and NPA analysis have been investigated in this part of the research [55]. The Fukui function summarized for an atom within a molecule suggested by Yang and Mortier [56] were expressed in the following terms:

$$\text{Term corresponding to nucleophilic aggression}: f_k^+ = [q_k(N+1) - q_k(N)] \tag{11}$$

$$\text{Term corresponding to electrophilic aggression}: f_k^- = [q_k(N) - (N-1)] \tag{12}$$

Atomic charges based on Hirshfeld charges, Fukui functions (f_k^+, f_k^-), Mulliken and Natural population analysis (NPA) for BFDP molecule sites using CAM−B3LYP at 6−311G++(d,p) level were presented in Table 6 Considering the terms mentioned previously, the

Table 5
Calculated energy values of BFDP by B3LYP/6−311G++(d,p) level of theory.

Parameters	Calculated energies
E (a.u.)	−1064.90
E_{HOMO} (eV)	−8.50
E_{LUMO} (eV)	0.13
$\left|\Delta E_{HOMO-LUMO}\right|$ (eV)	8.37
E_{HOMO-1} (eV)	−8.66
E_{LUMO+1} (eV)	0.19
$\left|\Delta E_{(HOMO-1)-(LUMO+1)}\right|$ (eV)	8.47
Dipole Moment (μ) (Debye)	1.08
Ionization potential (I)	8.50
Electron affinity (A)	−0.13
Electronegativity (χ)	4.19
Chemical potential (P)	−4.19
Chemical hardness (η)	4.32
Chemical softness (s)	2.16
Electrophilicity index (ω)	0.14
Hyper-hardness (Γ)	8.47

Table 6
Atomic charges based on Hirshfeld charges, Fukui functions (f_k^+, f_k^-), Mulliken and Natural population analysis (NPA) for BFDP molecule Sites using CAM−B3LYP at 6−311G++(d,p) level.

Atoms	Hirshfeld charges			Fukui indice		Mulliken	NPA
	Q(N)	Q (N-1)	Q (N+1)	f⁺	f⁻		
F1	−0.1019	−0.1230	−0.0549	0.0470	0.0211	−0.1789	−0.3575
F2	−0.1019	−0.1211	−0.0600	0.0419	0.0192	−0.1784	−0.3574
N1	−0.0712	−0.1123	−0.0594	0.0118	0.0411	0.2055	−0.6929
O1	−0.2607	−0.2905	−0.1400	0.1207	0.0298	−0.2330	−0.5593
C1	0.0581	−0.0351	0.0784	0.0203	0.0932	0.0099	−0.0198
C2	0.0332	−0.0108	0.0927	0.0595	0.0440	−0.1320	−0.4758
C3	0.1734	0.1579	0.2127	0.0393	0.0155	−0.1754	0.6167
C4	0.0067	0.0043	0.0238	0.0171	0.0024	0.1577	−0.1510
C5	0.0564	−0.0203	0.0733	0.0169	0.0767	0.2000	−0.0170
C6	−0.0080	−0.0153	0.0305	0.0385	0.0073	0.5280	−0.0589
C7	0.0098	−0.1149	0.0569	0.0471	0.1247	−0.1484	−0.1776
C8	0.0047	−0.0674	0.0653	0.0606	0.0721	0.0665	−0.2633
C9	0.0744	0.0538	0.1289	0.0545	0.0206	−0.4095	0.41437
C10	0.0047	−0.0414	0.0572	0.0525	0.0461	0.1216	−0.2611
C11	0.0098	−0.0216	0.0501	0.0403	0.0314	0.0541	−0.1819
C12	−0.0060	−0.0106	0.0231	0.0291	0.0046	0.5750	−0.0598
C13	0.0130	−0.0040	0.0433	0.0303	0.0170	0.0196	−0.1864
C14	0.0037	−0.0331	0.0523	0.0486	0.0368	−0.0845	−0.2632
C15	0.0742	0.0563	0.1220	0.0478	0.0179	−0.4392	0.4156
C16	0.0044	−0.0595	0.0559	0.0515	0.0639	0.0764	−0.2674
C17	0.0139	−0.0864	0.0534	0.0395	0.1003	0.0848	−0.1765
C18	0.0094	−0.0282	0.0510	0.0416	0.0376	−0.1173	−0.5871
C19	−0.0007	−0.0775	0.0424	0.0431	0.0768	−0.0027	−0.5871
H1	0.0304	−0.0005	0.0001	−0.0303	0.0309	0.1667	0.1723
H2	0.0501	−0.0006	−0.0004	−0.0505	0.0507	0.1775	0.2301
H3	0.0494	−0.0001	−0.0010	−0.0504	0.0495	0.2339	0.2341
H4	0.0288	−0.0007	0.0005	−0.0283	0.0295	0.2485	0.1784
H5	0.0522	−0.0004	−0.0005	−0.0527	0.0526	0.1692	0.2114
H6	0.0615	−0.0004	−0.0003	−0.0618	0.0619	0.2138	0.2275
H7	0.0610	−0.0002	0.0000	−0.0610	0.0612	0.2116	0.2265
H8	0.0506	−0.0004	−0.0007	−0.0513	0.0510	0.1859	0.2219
H9	0.0515	−0.0000	−0.0004	−0.0519	0.0515	0.1809	0.2246
H10	0.0609	−0.0000	0.0001	−0.0608	0.0609	0.2162	0.2267
H11	0.0614	−0.0000	−0.0000	−0.0614	0.0614	0.2217	0.2308
H12	0.0528	−0.0000	−0.0005	−0.0533	0.0528	0.1630	0.2128
H13	0.0336	0.0001	0.0000	−0.0336	0.0335	0.1669	0.2131
H14	0.0389	0.0004	0.0011	−0.0378	0.0335	0.1624	0.2165
H15	0.0415	0.0001	0.0009	−0.0406	0.0414	0.1947	0.2138
H16	0.0405	−0.0002	−0.0001	−0.0406	0.0407	0.1920	0.2263
H17	0.0333	−0.0002	0.0000	−0.0333	0.0335	0.1418	0.2086
H18	0.0355	−0.0002	0.0000	−0.0355	0.0357	0.1695	0.2096
H19	0.1080	−0.0001	−0.0003	−01083	0.1083	0.2475	0.3695

relatively higher degree of reactivity descriptors (f_k^+) found around the O1 atom indicates the highest potential for nucleophilic attack at this particular location. In contrast, the relative local reactivity descriptors (f_k^-) at C1, C7 and C17 suggest that these sites may be the easiest candidates for electrophilic attack. According to the Hirshfeld, Mulliken and natural population analysis charges, F1, F2, N1 and O1 atoms display significant negative atomic loads in the crystalline compound having the following amounts of CAM-B3LYP functional values: 0.1019, −0.1019, −0.0712 and −0.2607/−0.1789, −0.1784, 0.2055 and −0.2330/−0.3575, −0.3574, −0.6929 and −0.5593, respectively. That might be due to the hydrogen atoms linkage in these locations. The atoms of carbon have a positive or negative charge depending on their position in the BFDP molecule. All atoms of hydrogen carry net positive charges for the Hirshfeld, Mulliken and natural population analysis loadings. These data generally match well with the molecule electrostatic potential (MEP) chart.

3.12. Thermodynamic characteristics

In this investigation, we studied the thermodynamic characteristics, mainly enthalpy (H), entropy (S) and heat capacities (C), which show a remarkable increase with the elevation of the temperature that, are depicted in Fig. S10. The measurements in the table and the figure were determined from the harmonic frequency results. Thermodynamic characteristics of the BFDP compound were computed in gas phase, pressure of 1 atm and 298.15 K of temperature. The enthalpy (H), entropy (S) and heat capacities (C) increases could be caused directly related to the effect of the temperature rise on the vibration, translation, rotation and electronic sources of energy [57]. The values of thermodynamical characteristics of gas phase BFDP compound are collected in Table 7. The tabulated information reveals that the zero-point correction, energy values, and enthalpy thermal correction were smallest with the

Table 7
Thermodynamical characteristics of gas phase BFDP compound.

Characteristics	CAM−B3LYP	WB97XD
Zero-point vibrational energy (Joules/Mol)	902484.2	215.84612
Zero-point correction (Hartree/Particle)	0.343738	0.343973
Thermal correction to Energy	0.363542	0.363615
Thermal correction to Enthalpy	0.364486	0.364560
Thermal correction to Gibbs Free Energy	0.294230	0.294834
Sum of electronic and zero-point Energies	−1064.556605	−1064.736617
Sum of electronic and thermal Energies	−1064.536801	−1064.716975
Sum of electronic and thermal Enthalpies	−1064.535857	−1064.716030
Sum of electronic and thermal Free Energies	−1064.606114	−1064.785756
Energies E (Thermal) (kCal/Mol)		
Total	228.126	228.172
Electronic	0.000	0.000
Translational	0.889	0.889
Rotational	0.889	0.889
Cv (Cal/Mol.Kelvin)		
Total	78.426	78.276
Electronic	0.000	0.000
Translational	2.981	2.981
Rotational	2.981	2.981
S (Cal/Mol.Kelvin)		
Total	147.868	146.751
Electronic	0.000	0.000
Translational	43.140	43.140
Rotational	35.295	35.282

DFT/CAM−B3LYP 6−311G++ (d,p) base set applied.

3.13. Thermal property

TGA/DTA curve of BFDP, recorded in the range of 28–500 °C under nitrogen atmosphere is shown in Fig. 9. A slight weight loss (2.2 %) was observed in between 30 and ~180 °C, which was due to the removal of surface adsorbed water molecules. It can also be inferring that BFDP was thermally stable up to ~180 °C. But, about 96 % weight losses are obtained in between 180 and 270 °C, indicating a complete degradation of BFDP. This result was also reveals that the BFDP has a one-step degradation process. In DTA curve, an endothermic peak at 113 °C can be assigned to removal of surface adsorbed water molecules [58]. A weak endothermic peak at ~263 °C was ascribed to the thermal degradation of BFDP. The results of TGA curve are well agreed with the DTA curve of BFDP.

3.14. Pass and molecular docking analysis

Prediction of Activity Spectra (PASS) can predict various classes of activity according to the composition of the molecular component. PASS testing of 2,6-bis(4-fluorophenyl)-3,3-dimethylpiperidin-4-one indicates the first antidyskinetic activity with 0.772 probability of being active (pa). Table 8 shows the highest probabilities of being active with the BFDP ligand. In Table 9, Pi represents the probability of being inactive with respect to various affinity binding estimates of the ligand positions determined by Autodock Vina program [23]. The Pass tool proposes dyskinesia PDB-ID: 3HP7 Putative hemolysin from Streptococcus thermophiles as the main active probability with 2.50 Å of XRD resolution method [59]. This disease is a major complication of Parkinson's disease. The investigated BFDP ligand has −8.9 kcal/mol with 3HP7 protein, −6.6 kcal/mol with 4LK5 and -4.2 Kcal/molagainst 5C5S proteins. The three proteins has a better rsolution ≤2.5 Å, 4LK5enoyl-CoA hydratase protein has a resolution of 1.53 Å using X-ray diffraction technique. As well as 2.20 Å for 5C5S human Myosin 9b RhoGAP protein. The free energetic binding value for every protein/ligand combination was clearly negative, indicating a potential inhibitor of 7HP5 dyskinetic, 5C5S lung cancer and 4LK5 non-tuberculous mycobacteria causing 2 types of human infections towards the BFDP ligand [60]. Fig. 10 shows 3D and 2D ligand-aminoacids proteins interactions (A)7HP5 protein with BFDP; (B) 5C55 with BFDP; (C) 4LK5 with BFDP. The ligand is binding to the active sites of the protein. The following interactions are occurring: conventional hydrogen bonding, Alkyl, carbon hydrogen bonding, Pi-Alkyl, T-shaped Pi-Pi, stacked Pi-Pi, Pi-Donor hydrogen bonding and halogen bonding. Each protein connects to the ligand at a defined distance (Table 10). These results lead us to consider that the BFDP substance could display potential inhibitory activity against Hydratase, Enoyl-CoA hydratase protein and human Myosin 9b RhoGAP and act as a target agent for Parkinson's disease, lung cancer and human infectious illnesses.

3.15. In silico ADMET study

In addition to problems with safety and effectiveness, wrong pharmacokinetic properties made several powerful compounds useless as medicines. ADME characteristics are determinants of biological compounds drugg ability. In this study, the SwissADME database was used to predict the physicochemical and pharmacokinetic parameters of the target substances [61]. In conclusion, five different
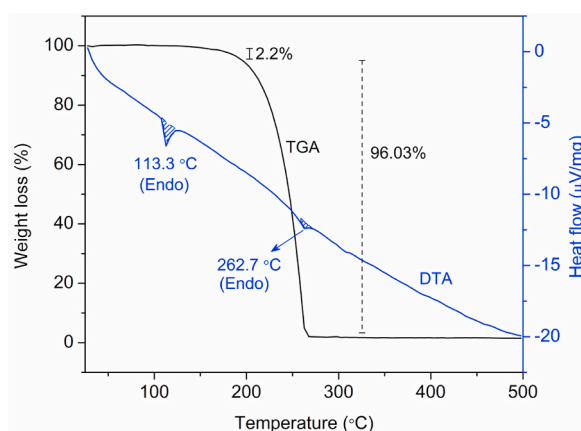
Fig. 9. TGA/DTA analysis of BFDP.

Table 8
PASS prediction activity of BFDP molecule.

Pa	Pi	Activity
0.740	0.011	Antidyskinetic
0.740	0.042	Testosterone 17beta-dehydrogenase (NADP+) inhibitor
0.733	0.022	5 Hydroxytryptamine release stimulant
0.714	0.031	Nicotinic alpha6beta3beta4alpha5 receptorantagonist
0.666	0.062	CYP2J substrate
0.626	0.042	Nicotinic alpha2beta2 receptorantagonist
0.602	0.046	Phosphatase inhibitor
0.596	0.006	5 Hydroxytryptamineuptake stimulant
0.596	0.020	Vasoprotector
0.561	0.095	Nootropic

Table 9
Auto Dock Vina findings of the binding affinity and RMSD values of several poses in the 3HP7 inhibitor of BFDP compound.

	3HP7			4LK5			5C5S		
Mode	Affinity (Kcal/mol)	RMS dl.b.	Rmsdu.b	Affinity (Kcal/mol)	RMS dl.b.	Rmsdu.b	Affinity (Kcal/mol)	RMS dl.b.	Rmsdu.b
1	−8.9	0.00	0.00	−6.6	0.00	0.00	−4.2	0.000	0.000
2	−8.3	3.09	4.618	−6.6	3.046	6.557	−3.7	2.761	7.254
3	−8.1	2.809	4.053	−6.2	2.927	4.357	−3.5	3.347	5.006
4	−8.0	0.756	6.547	−6.0	3.741	7.901	−3.5	1.976	6.449
5	−7.7	3.490	4.332	−5.9	4.961	7.919	−3.5	3.458	7.394
6	−7.6	1.863	2.336	−5.8	3.296	4.750	−3.3	2.939	7.548
7	−7.6	3.169	6.717	−5.6	17.997	18.860	−3.2	3.003	3.849
8	−7.5	3.541	6.570	−5.6	17.268	19.258	−3.2	2.076	2.718
9	−7.4	2.679	7.460	−5.5	5.403	7.831	−3.2	1.970	2.666

models predict lipophilicity: MLOGP, WLOGP, SILICOS-IT, XLOGP3 and iLOGP. Its arithmetic mean yields the consensus log $P_{o/w}$ [62]. Bioavailability radar is a picture of six physicochemical parameters, such as size, lipophilicity, polarity, solubility, saturation, and flexibility [63,64]. The middle pink hexagon shows the optimal bioavailability zone for oral administration. Based on these calculations, the molecule of interest (BFDP) had good qualities, as shown in Table 11. Based on the data, the BFDP compound satisfies the conditions of Lipinski's rule of five exactly.

The BFDP oral bioavailability radar pattern is depicted in Fig. 11(A) The BFDP compound has two bonds that are rotatable. It is an important way to measure how flexible a molecule is, and it must be less than 10. The BOILED-Egg is a promising model for prediction based on the polarity predictions of lipophilicity and small molecules. BOILED-Egg is a combination of polarity shown in TPSA versus lipophilicity represented in WLOGP, another approach for predicting lipophilicity. The white part of the BOILED Egg graph indicates the potential for GI absorption, whereas the yolk portion indicates the potential for BBB permeability [65]. The tPSAVs WLOGP plot (BOILED-Egg) of the BFDP compounds is depicted in Fig. 11(B) The higher levels of gastrointestinal absorption (GI) and skin permeability (Log Kp = −5.78 cm/s), as well as the known BBB penetration data, indicating that the CEFP compound may be a feasible treatment alternative.
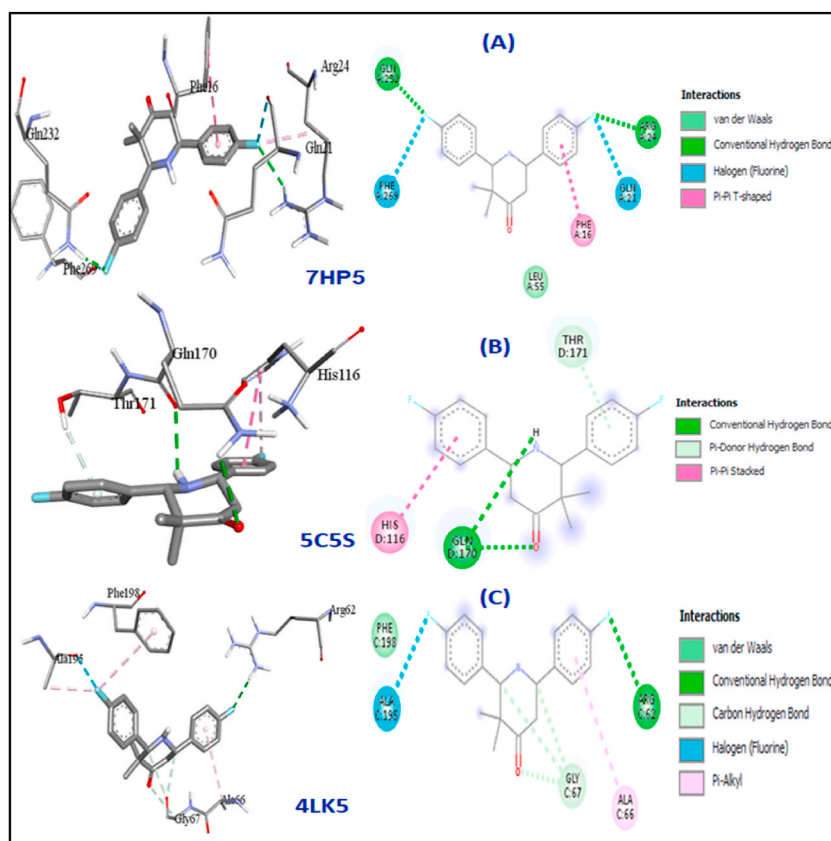
Fig. 10. 3D and 2D ligand-aminoacids proteins interactions (A)7HP5 protein with BFDP; (B) 5C55 with BFDP; (C) 4LK5 with BFDP.

Table 10
Intermolecular interaction was developed from the residues of the three proteins PDB ID: 4LK5, 3HP7, and 5C5S towards the BFDP ligand.

Protein/PDB-ID	Residues	Compound part	Types	Category	Distance (Å)
Enoyl-CoA hydratase protein/4LK5	C: ALA66	Ring 1	Pi-Alkyl	Hydrophobic	5488
	C: GLY 67	C5	CarbonHydrogen Bond	Hydrogen Bond	3473
	C: GLY 67	C1	CarbonHydrogen Bond	Hydrogen Bond	3265
	C: GLY 67	O1	CarbonHydrogen Bond	Hydrogen Bond	3488
	C: ARG62	F2	Conventional Hydrogen Bond; Halogen (Fluorine)	HydrogenBond; Halogen	2774
	C: ALA195	F1	Halogen (Fluorine)	Halogen	3036
Hydratase protein/3HP7	A: PHE 269	F1	Halogen (Fluorine)	Halogen	3516
	A:GLN232	F1	ConventionalHydrogenBond; Halogen (Fluorine)	HydrogenBond; Halogen	2150
	A: LEU 55	H2B	Alkyl	Hydrophobic	5093
	A: PHE 16	Ring 1	Pi-Pi T-shaped	Hydrophobic	4766
	A: GLN 21	F2	Halogen (Fluorine)	Halogen	2897
	A: ARG 24	F2	ConventionalHydrogenBond; Halogen (Fluorine)	HydrogenBond; Halogen	2647
Human Myosin 9b RhoGAP/5C5S protein	D: GLN 170	O1	ConventionalHydrogen Bond	HydrogenBond	3019
	D: HIS 116	Ring 1	Pi-PiStacked	Hydrophobic	4147
	D: GLN 170	H1N	ConventionalHydrogen Bond	Hydrogen Bond	2735
	D: THR 171	Ring 2	Pi-DonorHydrogen Bond	Hydrogen Bond	2746

Ring 1: C12–C13–C14–C15–C16; Ring 2: C6–C7–C8–C9–C10–C11.

Table 11

Pharmacokinetic properties and Physicochemical of BFDP molecule.

ADME Parameters	Values
Formula	$C_{19}H_{19}F_2NO$
Molecular weight	315.36 g/mol
FLEX (Flexibility) Number of rotatable bonds	2
Num. heavy atoms	23
Number of H-bond acceptors	4
Number of H-bond donors	1
Molar Refractivity	89.20
TPSA (Polarity)	29.10 Å^2
Log Po/w (iLOGP) (Lipophilicity)	3.04
Consensus Log $P_{o/w}$ (Lipophilicity)	3.89
POLAR (Polarity)	Poorly soluble
GI absorption	High
Blood Brain Barrier (BBB) Permeability	Yes
CYP1A2 inhibitor	No
CYP2C19 inhibitor	Yes
CYP2C9 inhibitor	No
CYP2D6 inhibitor	Yes
CYP3A4 inhibitor	Yes
Log K_p (skin permeation)	−5.78 cm/s
Lipinski	Yes; 0 violation
Ghose, Veber, Egan, and Muegge	Yes
Bioavailability Score	0.55
Synthetic accessibility	2.75
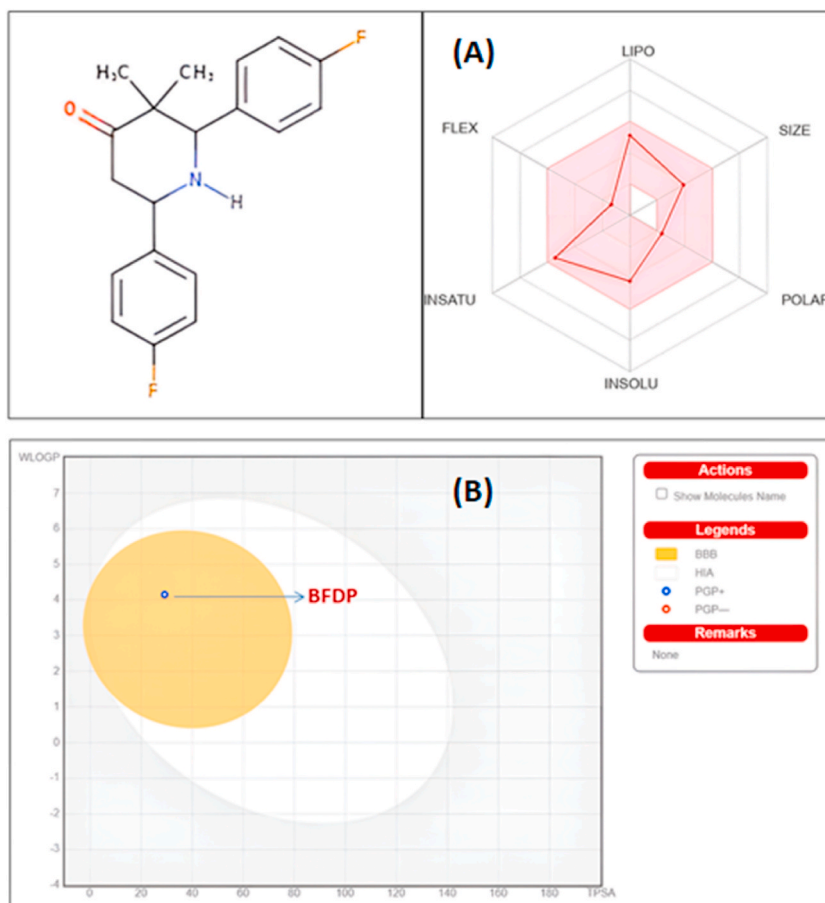
Fig. 11. (A) Oral bioavailability radar diagram and (B) BOILED-Egg diagram of BFDP.

4. Conclusions

BFDP was synthesised and characterised using FT-IR, mass spectra and ^{1}H NMR, ^{13}C NMR spectroscopy. The DFT, density functional theory and B3LYP/6-311G++ (d,p) level of theory was used for optimization, vibrational analysis, and theoretical calculations for the BFDP compound. Furthermore, theoretical structural elements such as bond angle and bond length complemented the actual and calculated geometrical characteristics of the BFDP compound. According to the spectrum data, the axial lone pair of electrons upon nitrogen in BFDP was projected to enrich the anti-periplanar axial hydrogen atoms at the two alpha positions in this conformationally rigid piperidine structure. This finding provides support for the chair conformation that defines the piperidine ring in BFDP, with the lone pair of electrons situated axially. The Hirshfeld analysis was performed to better understand the interatomic interaction, molecular structure, and hydrogen bonding of the BFDP molecule. The most common interactions among molecules are H⋯H, H⋯F/F⋯H, C⋯H/H⋯C accounting for 50.4 %, 20.0 %, and 14.3 %, respectively, for the Hirshfeld surface. Electronic properties such as global quantum descriptors and HOMO and LUMO energies were also studied, and a theoretical energy gap of −8.37 eV was found. The significant mode of vibration was also studied using theoretical values and vibrational frequencies were compared to the actual results. F1, F2, N1, and O1 atoms exhibit significant negative atomic loads in the crystalline compound with the following CAM-B3LYP functional values: 0.1019, −0.1019, −0.0712, and −0.2607; −0.1789, −0.1784, 0.2055, and −0.2330; −0.3575, −0.3574, −0.6929, and −0.5593, respectively. Second-order hyperpolarizabilities are high for CAM-B3LYP and WB97XD, with values of 23.7748 × 10^{-36} and 23.6396 × 10^{-36} esu, respectively. It demonstrates that the BFDP crystal is an ideal compound for nonlinear optical materials. Thermodynamic properties of the BFDP compound were calculated in the gas phase at 1 atm of pressure and 298.15 K of temperature. The thermal property was also tested, and the TGA curve findings correspond well with the BFDP DTA curve. The BFDP compound was molecular docked, and the results indicate that it may have potential inhibitory activity against Hydratase, Enoyl-CoA hydratase protein, and human Myosin 9b RhoGAP, as well as act as a target agent for Parkinson's disease, lung cancer, and human infectious diseases. Furthermore, the BFDP molecule was evaluated for drug-likeness employing Lipinski's five requirements as well as ADMET experiments. The results show that the BFDP has strong pharmacological characteristics and has high potential as a medicine. We believe that our findings will help to illuminate future theoretical and experimental research employing analogous structures.

Data availability statement

Data included in article/supplementary material/referenced in article.

Supplementary material

Supplementary content related to this article has been published online.

CRediT authorship contribution statement

Thangamani Arumugam: Conceptualization, Funding acquisition, Investigation, Methodology, Writing – original draft. **Arulraj Ramalingam:** Conceptualization, Formal analysis, Investigation, Methodology, Writing – review & editing. **Guerroudj Ahlam Roufieda:** Formal analysis, Investigation, Resources. **Sivakumar Sambandam:** Methodology, Supervision. **Boukabcha Nourdine:** Software, Visualization. **Chouaih Abdelkader:** Data curation, Validation.

Declaration of competing interest

The authors declare that they have no known competing financial interests or personal relationships that could have appeared to influence the work reported in this paper.

Acknowledgement

Appendix A. Supplementary data

Supplementary data to this article can be found online at https://doi.org/10.1016/j.heliyon.2023.e21315.

References

[1] A. Nazem, G.A. Mansoori, Nanotechnology solutions for Alzheimer's disease: advances in research tools, diagnostic methods and therapeutic agents, J. Alzheim. Dis. 13 (2) (2008) 199–223, https://doi.org/10.3233/JAD-2008-13210.

[2] M. Srikanth, J.A. Kessler, Nanotechnology-novel therapeutics for CNS disorders, Nat. Rev. Neurol. 8 (6) (2012) 307–318, https://doi.org/10.1038/nrneurol.2012.76.

[3] N. Aguilar, B. Garcia, M. Cunningham, S. David, Synthesis of a Parkinson's disease treatment drug, the R,R-tartrate salt of R-Rasagiline: a three week introductory organic chemistry lab sequence, J. Chem. Educ. 93 (5) (2016) 937–940, https://doi.org/10.1021/acs.jchemed.5b00357.

[4] P. Rusek, M. Wala, M. Druszczyńska, M. Fol, Infectious agents as stimuli of trained innate immunity, Int. J. Mol. Sci. 19 (2) (2018) 456, https://doi.org/10.3390/ijms19020456.

[5] L. Zhu, Y. Wang, W. Lv, X. Wu, H. Sheng, C. He, J. Hu, Schizandrin A can inhibit non-small cell lung cancer cell proliferation by inducing cell cycle arrest, apoptosis and autophagy, Int. J. Mol. Med. 48 (6) (2021) 214, https://doi.org/10.3892/ijmm.2021.5047.

[6] R. Arulraj, M. Nurulhuda, W.J. Chng, M. Mouna, S. Sivakumar, I. Noureddine, 3-Chloro-3-methyl-2,6-diarylpiperidin-4-ones as Anti-cancer agents: synthesis, biological evaluation, molecular docking, and in silico ADMET prediction, Biomolecules 12 (8) (2022) 1093, https://doi.org/10.3390/biom12081093.

[7] J. Jayabharathi, A. Thangamani, M. Padmavathy, B. Krishnakumar, Synthesis and microbial evaluation of novel N(1)-Arilidene-N(2)-t(3)-methyl-r(2),c(6)-diaryl-piperidin-4-one azine derivatives, Med. Chem. Res. 15 (2007) 431–442, https://doi.org/10.1007/s00044-006-0014-0.

[8] R. Arulraj, S. Sivakumar, M. Mouna, A.D. Omar, I. Noureddine, M.J. Wojcik, Study of a new piperidone as an anti-Alzheimer agent: molecular docking, electronic and intermolecular interaction investigations by DFT method, J. King Saud Univ. Sci. 33 (8) (2021), 101632, https://doi.org/10.1016/j.jksus.2021.101632.

[9] A. Thangamani, Synthesis and biological activities of some 3,5-diaryl-N-hydroxy-tetrahydro1,4-thiazine-1,1-dioxides, J. Appl. Adv. Res. 1 (4) (2016) 8–13, https://doi.org/10.21839/jaar.2016.v1i4.36.

[10] R. Arulraj, A.R. Guerroudj, S. Sivakumar, K. Anitha, K. Rajkumar, B. Nourdine, A. Chouaih, E. Manikandan, Synthesis, vibrational spectra, Hirshfeld surface analysis, DFT calculations, and in silico ADMET study of 3-(2-chloroethyl)-2,6-bis(4-fluorophenyl)piperidin-4-one: a potent anti-Alzheimer agent, J. Mol. Struct. 1269 (2022), 133845, https://doi.org/10.1016/j.molstruc.2022.133845.

[11] A. Ramalingam, S. Sambandam, H. Louis, A. Imojara, G.E. Mathias, Spectroscopic study, Hirshfeld surface, DFT, in-silico molecular docking and ADMET studies of 2,6-bis(4-chlorophenyl)-3-isopropylpiperidin-4-one (BCIP): a potent antiviral agent, J. Mol. Struct. 1291 (2023), 135912, https://doi.org/10.1016/j.molstruc.2023.135912.

[12] A. Dhandapani, S. Veeramanikandan, R.S. Kumar, A.I. Almansour, N. Arumugam, S. Subashchandrabose, J. Suresh, R. Arulraj, D. Gajalakshmi, Synthesis, in vitro and in silico antitumor evaluation of 3-(2,6-dichlorophenyl)-1,5-diphenylpentane-1,5-dione: structure, spectroscopic, RDG, Hirshfeld and DFT based analyses, J. Mol. Struct. 1251 (2022), 132002, https://doi.org/10.1016/j.molstruc.2021.132002.

[13] R. Arulraj, S. Sivakumar, S. Suresh, K. Anitha, Synthesis, Vibrational spectra, DFT calculations, Hirshfeld surface analysis and Molecular docking study of 3-chloro-3-methyl-2,6-diphenylpiperidin-4-one, Spectrochim. Acta-A: Mol. Biomol. Spectrosc. 232 (2020), 118166, https://doi.org/10.1016/j.saa.2020.118166.

[14] G.M. Sheldrick, A. Short history of Shelx, Acta Crystallogr. A 64 (2008) 112–122, https://doi.org/10.1107/S0108767307043930.

[15] G.M. Sheldrick, Crystal structure refinement with SHELXL, Acta Crystallogr. A 71 (2015) 3–8, https://doi.org/10.1107/S2053229614024218.

[16] L.J. Farrugia, WinGX and ORTEP for windows–an update, J. Appl. Crystallogr. 45 (2012) 849–854, https://doi.org/10.1107/S0021889812029111.

[17] W. Kohn, A.D. Becke, R.G. Parr, Density functional theory of electronic structure, J. Phys. Chem. 100 (31) (1996) 12974–12980, https://doi.org/10.1021/jp960669l.

[18] M.J. Frisch, G.W. Trucks, H.B. Schlegel, G.E. Scuseria, M.A. Robb, J.R. Cheeseman, G. Scalmani, V. Barone, B. Mennucci, G.A. Petersson, H. Nakatsuji, M. Caricato, X. Li, H.P. Hratchian, A.F. Izmaylov, J. Bloino, G. Zheng, J.L. Sonnenberg, M. Hada, M. Ehara, K. Toyota, R. Fukuda, J. Hasegawa, M. Ishida, T. Nakajima, Y. Honda, O. Kitao, H. Nakai, T. Vreven, J.A. Montgomery Jr., J.E. Peralta, F. Ogliaro, M. Bearpark, J.J. Heyd, E. Brothers, K.N. Kudin, V. N. Staroverov, R. Kobayashi, J. Normand, K. Raghavachari, A. Rendell, J.C. Burant, S.S. Iyengar, J. Tomasi, M. Cossi, N. Rega, J.M. Millam, M. Klene, J.E. Knox, J.B. Cross, V. Bakken, C. Adamo, J. Jaramillo, R. Gomperts, R.E. Stratmann, O. Yazyev, A.J. Austin, R. Cammi, C. Pomelli, J.W. Ochterski, R.L. Martin, K. Morokuma, V.G. Zakrzewski, G.A. Voth, P. Salvador, J.J. Dannenberg, S. Dapprich, A.D. Daniels, E.O. Farkas, J.B. Foresman, J.V. Ortiz, J. Cioslowski, D. J. Fox, Gaussian 09, Gaussian Inc, Wallingford, CT, 2009.

[19] A. Frisch, A.B. Nielson, A.J. Holder, GAUSSVIEW User Manual, Gaussian Inc, Pittsburgh, 2000.

[20] M.H. Jamroz, Vibrational Energy Distribution Analysis VEDA, vol. 4, Warsaw, 2004.

[21] A. Kumar, S. Sambandam, A. Ramalingam, R. Krishnamoorthy, D. Arumugam, O.E. Oyeneyin, Synthesis, molecular docking of 3-(2-chloroethyl)-2,6-diphenylpiperidin-4-one: Hirshfeld surface, spectroscopic and DFT based analyses, J. Mol. Struct. 1262 (2022), 132993, https://doi.org/10.1016/j.molstruc.2022.132993.

[22] P.R. Spackman, M.J. Turner, J.J. McKinnon, S.K. Wolff, D.J. Grimwood, D. Jayatilaka, M.A. Spackman, CrystalExplorer: a program for Hirshfeld surface analysis, visualization and quantitative analysis of molecular crystals, J. Appl. Crystallogr. 54 (3) (2021) 1006–1011, https://doi.org/10.1107/S1600576721002910.

[23] O. Trott, A.J. Olson, AutoDock Vina, Improving the speed and accuracy of docking with a new scoring function, efficient optimization, and multithreading, J. Comput. Chem. 31 (2) (2010) 455–461, https://doi.org/10.1002/jcc.21334.

[24] Dassault Systèmes Biovia, Discovery Studio Modeling Environment, Dassault Systèmes, San Diego, 2020. Release v21.1.0.20.29.8.

[25] C.R. Noller, V. Baliah, The preparation of some piperidine derivatives by the Mannich reaction, J. Am. Chem. Soc. 70 (11) (1948) 3853–3855, https://doi.org/10.1021/ja01191a092.

[26] R. Arulraj, S. Sivakumar, A. Thiruvalluvar, A. Manimekalai, X-Ray crystal structure, molecular structure, spectral and antimicrobial activity of t-(3)-benzyl-r-(2), c-(6)-diphenylpiperidin-4-one, Chem. Sci. Rev. Lett. 5 (18) (2016) 99–105. https://scholarbank.nus.edu.sg/handle/10635/165299.

[27] A. Manimekalai, S. Sivakumar, Synthesis, spectral and computational studies of some N-acyl-t(3)-isopropyl-r(2),c(6)-bis-2′-furylpiperidin-4-one oximes, Spectrochim. Acta-A: Mol. Biomol. Spectrosc. 75 (1) (2010) 113–120, https://doi.org/10.1016/j.saa.2009.09.051.

[28] R. Arulraj, S. Sivakumar, A. Thiruvalluvar, A. Manimekalai, t-3-Benzyl-r-2,c-6-diphenylpiperidin-4-one, IUCrData 1 (2) (2016) x160188, https://doi.org/10.1107/S2414314616001887.

[29] R. Arulraj, S. Sivakumar, A. Thiruvalluvar, M. Kaur, J.P. Jasinski, 3-Chloro-r-2,c-6-bis(4-fluorophenyl)-3-methylpiperidin-4-one, IUCrData 1 (10) (2016) x161580, https://doi.org/10.1107/S2414314616015807.

[30] R. Arulraj, S. Sivakumar, A. Thiruvalluvar, A. Manimekalai, Crystal Structure of t-3-Benzyl-r-2,c-6-diphenylpiperidin-4-one oxime, IUCrData 1 (12) (2016) x161982, https://doi.org/10.1107/S2414314616019829.

[31] K. Rajkumar, S. Sivakumar, R. Arulraj, M. Kaur, J.P. Jasinski, A. Manimekalai, A. Thiruvalluvar, Crystal structures of two new 3-(2-chloroethyl)-r(2),c(6)-diarylpiperidin-4-ones, Acta Crystallogr. E74 (4) (2018) 483–486.

[32] R. Arulraj, S. Sivakumar, M. Kaur, A. Thiruvalluvar, J.P. Jasinski, Crystal structures of three 3-chloro-3-methyl-2,6-diarylpiperidin-4-ones, Acta Crystallogr. E Crystallogr. Commun. 73 (2) (2017) 107–111, https://doi.org/10.1107/S2056989016020661.

[33] A. Manimekalai, S. Sivakumar, Synthesis, spectral and conformational studies of some N-arylsulfonyl-t(3)-isopropyl-r(2),c(6)-diarylpiperidin-4-ones, Magn. Reson. Chem. Letters 49 (12) (2011) 830–834, https://doi.org/10.1002/mrc.2829.

[34] A. Thangamani, Synthesis and conformational study of some N-nitroso-t(3)-benzyl-r(2),c(6)-bis(aryl)piperidin-4-one oximes using NMR spectra, J. Mol. Struct. 1221 (2020), 128810, https://doi.org/10.1016/j.molstruc.2020.128810.

[35] R. Arulraj, S. Kansız, N. Dege, S. Sivakumar, Synthesis, crystal structure, DFT calculations and Hirshfeld surface analysis of 3-chloro-2,6-bis(4-chlorophenyl)-3-methylpiperidin-4-one, J. Chem. Crystallogr. 51 (2) (2021) 273–287, https://doi.org/10.1007/s10870-020-00852-3.

[36] M.A. Spackmann, D. Jayatilaka, Hirshfeld surface analysis, CrystEngComm 11 (2009) 19–32, https://doi.org/10.1039/B818330A.

[37] M.A. Spackman, J.J. McKinnon, Fingerprinting intermolecular interactions in molecular Crystals, CrystEngComm 4 (2002) 378–392, https://doi.org/10.1039/B203191B.

[38] R. Arulraj, Hirshfeld surface analysis, interaction energy calculation and spectroscopical study of 3-chloro-3-methyl-r(2),c(6)-bis(p-tolyl)piperidin-4-one using DFT approaches, J. Mol. Struct. 1248 (2022), 131483, https://doi.org/10.1016/j.molstruc.2021.131483.

[39] G. Sofian, I. Noureddine, R. Thierry, M. Houda, Synthesis, experimental and computational study of a non-centrosymmetric material 3-methylbenzylammonium trioxonitrate, J. Mol. Struct. 1225 (2021), 129132, https://doi.org/10.1016/j.molstruc.2020.129132.

[40] M. Jemai, M. Khalfi, N. Issaoui, T. Roisnel, A.S. Kazachenko, O. Al-Dossary, H. Marouani, A.S. Kazachenko, Y.N. Malyar, Role of non-covalent interactions in novel supramolecular compound, bis(4-phenylpiperazin-1-ium) oxalate dihydrate: synthesis, molecular structure, thermal characterization, spectroscopic properties and quantum chemical study, Crystals 13 (6) (2023) 875, https://doi.org/10.3390/cryst13060875.

[41] T. Lu, F. Chen, Multiwfn: a multifunctional wave function analyzer, J. Comput. Chem. 33 (5) (2012) 580–592, https://doi.org/10.1002/jcc.22885.

[42] S. Ramkumar, R. Rajalakshmi, R. Arulraj, S. Sivakumar, P. Amalraj, A.R. Guerroudj, N. Boukabcha, A. Chouaih, Microwave assisted synthesis, vibrational spectra, Hirshfeld surface and interaction energy, DFT, topology, in silico ADMET and molecular docking studies of 1,2-bis(4-methoxybenzylidene)hydrazine, J. Mol. Struct. 1278 (2023) (2023), 134946, https://doi.org/10.1016/j.molstruc.2023.134946.

[43] P. Agarwal, S. Bee, A. Gupta, P. Tandon, V.K. Rastogi, S. Mishra, P. Rawat, Quantum chemical study on influence of intermolecular hydrogen bonding on the geometry, the atomic charges and the vibrational dynamics of 2,6-dichlorobenzonitrile, Spectrochim. Acta-A: Mol. Biomol. Spectrosc. 121 (2014) 464–482, https://doi.org/10.1016/j.saa.2013.10.104.

[44] A. Fazilath Basha, F. Liakath Ali Khan, S. Muthu, M. Raja, Computational evaluation on molecular structure (Monomer, Dimer), RDG, ELF, electronic (HOMO-LUMO, MEP) properties, and spectroscopic profiling of 8-Quinolinesulfonamide with molecular docking studies, Comput. Theor. Chem. 1198 (2021), 113169, https://doi.org/10.1016/j.comptc.2021.113169.

[45] P. Jayaprakash, P. Sangeetha, M.P. Mohamed, G. Vinitha, S. Muthu, M. Prakash, M.L. Caroline, Growth and characterization of dl-Mandelic acid ($C_6H_5CH(OH)CO_2H$) single crystal for third-order nonlinear optical applications, J. Mol. Struct. 1148 (2017) 314–321, https://doi.org/10.1016/j.molstruc.2017.07.049.

[46] M. Ashfaq, K.S. Munawar, G. Bogdanov, A. Ali, M.N. Tahir, G. Ahmed, R. Arulraj, M.M. Alam, M. Imran, S. Sivakumar, B. Munir, Single crystal inspection, Hirshfeld surface investigation and DFT study of a novel derivative of 4-fluoroaniline: 4-((4-fluorophenyl)amino)-4-oxobutanoic acid (BFAOB), J. Iran. Chem. Soc. 19 (5) (2022) 1953–1961, https://doi.org/10.1007/s13738-021-02432-4.

[47] A.R. Guerroudj, N. Boukabcha, A. Benmohammed, N. Dege, N.H. Belkafouf, N. Khelloul, A. Djafri, A. Chouaih, Synthesis, crystal structure, vibrational spectral investigation, intermolecular interactions, chemical reactivity, NLO properties and molecular docking analysis on (E)-N-(4-nitrobenzylidene)-3-chlorobenzenamine: a combined experimental and theoretical study, J. Mol. Struct. 1240 (2021), 130589, https://doi.org/10.1016/j.molstruc.2021.130589.

[48] R. Arulraj, K. Murugavel, S. Sivakumar, M. Mouna, E.O. Oluwatoba, S. Amirthaganesan, I. Noureddine, D.O. Nathanael, Synthesis, spectroscopic, topological, Hirshfeld surface analysis, and anti-COVID-19 molecular docking investigation of isopropyl 1-benzoyl-4-(benzoyloxy)-2,6-diphenyl-1,2,5,6-tetrahydropyridine-3-carboxylate, Heliyon 8 (10) (2022), e10831, https://doi.org/10.1016/j.heliyon.2022.e10831.

[49] K. Anitha, S. Sivakumar, R. Arulraj, K. Rajkumar, O.E. Oyeneyin, Synthesis, molecular docking of 3-(2-chloroethyl)-2,6-diphenylpiperidin-4-one: Hirshfeld surface, spectroscopic and DFT based analyses, J. Mol. Struct. 1262 (2022), 132993, https://doi.org/10.1016/j.molstruc.2022.132993.

[50] J. George, J.C. Prasana, S. Muthu, T.K. Kuruvilla, S. Sevanthi, R.S. Saji, Spectroscopic (FT-IR, FT Raman) and quantum mechanical study on N-(2,6-dimethylphenyl)-2-{4-[2-hydroxy-3-(2-methoxyphenoxy)propyl]piperazin-1-yl}acetamide, J. Mol. Struct. 1171 (2018) 268–278, https://doi.org/10.1016/j.molstruc.2018.05.106.

[51] M.H. Jamroz, Vibrational Energy Distribution Analysis VEDA4, Warsaw, 2004.

[52] K. Anitha, S. Sivakumar, R. Arulraj, K. Rajkumar, M. Kaur, J.P. Jasinski, Synthesis, crystal structure, DFT calculations and Hirshfeld surface analysis of 3-butyl-2,6-bis(4-fluorophenyl)piperidin-4-one, Acta Crystallogr. E Crystallogr. Commun. 76 (5) (2020) 651–655, https://doi.org/10.1107/S2056989020004636.

[53] S. Muthu, G. Ramachandran, Spectroscopic studies (FTIR, FT-Raman and UV–Visible), normal coordinate analysis, NBO analysis, first order hyper polarizability, HOMO and LUMO analysis of (1R)-N-(prop-2-yn-1-yl)-2,3-dihydro-1H-inden-1-amine molecule by ab initio HF and density functional methods, Spectrochim. Acta-A: Mol. Biomol. Spectrosc. 121 (2014) 394–403, https://doi.org/10.1016/j.saa.2013.10.093.

[54] R. Arulraj, S. Sivakumar, K. Rajkumar, J.P. Jasinski, M. Kaur, A. Thiruvalluvar, Synthesis, crystal structure, DFT calculations and Hirshfeld surface analysis of 3-chloro-3-methyl-r(2),c(6)-bis(p-methoxyphenyl)piperidin-4-one, J. Chem. Crystallogr. 50 (2020) 41–51, https://doi.org/10.1007/s10870-018-0759-6.

[55] P. Fuentealba, C. Cárdenas, Chapter 14-On the Analysis of the Fukui Function, Elsevier, Chemical Reactivity, 2023, pp. 421–432, https://doi.org/10.1016/B978-0-32-390257-1.00021-8.

[56] W. Yang, W.J. Mortier, The use of global and local molecular parameters for the analysis of the gas-phase basicity of amines, J. Am. Chem. Soc. 108 (19) (1986) 5708–5711.

[57] S. Malik, M. Chandrasekhar, T.S. Krishna, V.K. Sharma, Thermodynamic properties of piperidine and cyclic alkanone mixtures, J. Therm. Anal. Calorim. 129 (2017) 1751–1765, https://doi.org/10.1007/s10973-017-6365-6.

[58] M. Mouna, I. Noureddine, G. Sofian, A.D. Omar, S.K. Aleksandr, M. Houda, M.J. Wojcik, Molecular modeling and biological activity analysis of new organic-inorganic hybrid: 2-(3,4-dihydroxyphenyl) ethanaminium nitrate, J. King Saud Univ. Sci. 33 (8) (2021), 101616, https://doi.org/10.1016/j.jksus.2021.101616.

[59] A. Lagunin, A. Stepanchikova, D. Filimonov, V. Poroikov, PASS: prediction of activity spectra for biologically active substances, Bioinformatics 16 (8) (2000) 747–748, https://doi.org/10.1093/bioinformatics/16.8.747.

[60] M. Morelli, F. Blandini, N. Simola, R.A. Hauser, A_{2A} Receptor antagonism and dyskinesia in Parkinson's disease, Parkinson's Dis. (2012) (2012) 1–8, https://doi.org/10.1155/2012/489853.

[61] http://www.swissadme.ch/.

[62] S.A. Wildman, G.M. Crippen, Prediction of physicochemical parameters by atomic contributions, J. Chem. Inf. Comput. Sci. 39 (5) (1999) 868–873, https://doi.org/10.1021/ci990307l.

[63] R. Rajalakshmi, R. Arulraj, D. Chinnaraja, S. Sivakumar, I. Noureddine, O.M. Al-Dossary, L.G. Bousiakoug, Catalytic multicomponent synthesis, biological evaluation, molecular docking, and in silico ADMET studies of some novel 3-alkyl indoles, J. King Saud Univ. Sci. 35 (2) (2023), 102475, https://doi.org/10.1016/j.jksus.2022.102475.

[64] P. Manjusha, J.C. Prasana, S. Muthu, B.F. Rizwana, Spectroscopic elucidation (FT-IR, FT-Raman and UV-visible) with NBO, NLO, ELF, LOL, drug likeness and molecular docking analysis on 1-(2-ethylsulfonylethyl)-2-methyl-5-nitro-imidazole: an antiprotozoal agent, Comput. Biol. Chem. 88 (2020), 107330, https://doi.org/10.1016/j.compbiolchem.2020.107330.

[65] A. Dania, V. Zoete, A BOILED-Egg to predict gastrointestinal absorption and brain penetration of small molecules, ChemMedChem 11 (11) (2016) 1117–1121, https://doi.org/10.1002/cmdc.201600182.